AWARD NUMBER: W81XWH-19-1-0322

TITLE: Mathematical Modeling of Hemodynamics in Trauma-Induced Shock and Closed- Loop Trauma Resuscitation

PRINCIPAL INVESTIGATOR: George C. Kramer

CONTRACTING ORGANIZATION:
University of
Texas Medical Branch, Galveston
301 University Blvd Galveston TX
77555-1102

REPORT DATE: **July 2020**

TYPE OF REPORT: **Annual**

PREPARED FOR: U.S. Army Medical Research and Materiel Command
Fort Detrick, Maryland 21702-5012

REPORT DOCUMENTATION PAGE

Form Approved
OMB No. 0704-0188

1. REPORT DATE *(DD-MM-YYYY)*	2. REPORT TYPE	3. DATES COVERED *(From - To)*
07/28/2020	Annual Progress	07-1-19 to 06-30-20

4. TITLE AND SUBTITLE
Mathematical Modeling of Hemodynamics in
Trauma-Induced Shock and Closed- Loop Trauma Resuscitation

5a. CONTRACT NUMBER

5b. GRANT NUMBER
W81XWH1910322

5c. PROGRAM ELEMENT NUMBER

6. AUTHOR(S)
George C Kramer, PhD
Dept. of Anesthesiology
UTMB
Galveston, Tx

5d. PROJECT NUMBER

5e. TASK NUMBER

5f. WORK UNIT NUMBER

7. PERFORMING ORGANIZATION NAME(S) AND ADDRESS(ES)
UTMB
301 University Blvd
Galveston TX 77555-1102

8. PERFORMING ORGANIZATION REPORT NUMBER

9. SPONSORING/MONITORING AGENCY NAME(S) AND ADDRESS(ES)
Congressionally Directed Medical Research Programs Office
US Army Medical Research and Materiel Command
301-619-7033, DSN 343

10. SPONSOR/MONITOR'S ACRONYM(S)

11. SPONSOR/MONITOR'S REPORT NUMBER(S)

12. DISTRIBUTION/AVAILABILITY STATEMENT
A - unlimited
Approved for Public Release;

13. SUPPLEMENTARY NOTES

14. ABSTRACT
Our long-term goal is to deliver automated closed-loop fluid and drug resuscitation systems for combat casualty and trauma care. We have prototyped and performed extensive animal studies of such systems for hemorrhagic shock and burn shock. However, animal studies alone may not be sufficient to demonstrate the safety of these systems. A key component to demonstrating the safety of these systems is to use mathematical models that describe the physiology of shock and its response to a full range of injuries and therapies. The focus of this grant is to establish such mathematical models. We performed 15 anesthetized swine studies of hemorrhagic shock and fluid therapy to achieve the data for modeling. We also

15. SUBJECT TERMS
Hemorrhage, Resuscitation, Hypovolemia, Shock, Burn Injury, Hypotension, Fluid, Pressors, Closed Loop, Fluid Therapy

16. SECURITY CLASSIFICATION OF:			17. LIMITATION OF ABSTRACT	18. NUMBER OF PAGES	19a. NAME OF RESPONSIBLE PERSON
a. REPORT	b. ABSTRACT	c. THIS PAGE			19b. TELEPHONE NUMBER *(Include area code)*
UU	UU	UU	SAR		

Standard Form 298 (Rev. 8/98)
Prescribed by ANSI Std. Z39.18

TABLE OF CONTENTS

Page

Introduction 5

Keywords 5

Accomplishments 5

Impact 18

Changes/Problems 18

Products 19

Participants & Other Collaborating Organizations 20

Special Reporting Requirements 22

Appendices 24

1. INTRODUCTION:

Our long-term goal is to deliver automated closed-loop fluid and drug resuscitation systems for combat casualty and trauma care. We have prototyped and performed extensive animal studies of such systems for hemorrhagic shock and burn shock. However, animal studies alone may not be sufficient to demonstrate the safety of these systems across the wide range of patient and clinical conditions they may need to be used in during critical care. The focus of this grant is to establish mathematical models as the foundation for the development and evaluation of closed-loop trauma resuscitation algorithms and demonstrate the utility of these models in the development and optimization of closed-loop resuscitation algorithms. We will 1) Develop mathematical models of trauma-induced shock and resuscitation specifically for developing and evaluating closed-loop resuscitation control algorithms. We perform animal studies to provide the key data to develop models. 2) Perform quantitative evaluation of mathematical models of trauma-induced shock and resuscitation. 3) Establish utility of the mathematical models by comparing in silico versus animal testing of closed-loop resuscitation algorithms. Future autonomous closed-loop resuscitation systems well validated with extensive in silico testing based on mathematical models will allow Medics, Corpsmen, Forward Surgical Teams and Combat Support Hospitals to apply resuscitation therapies equivalent to that of the best civilian trauma centers.

2. KEYWORDS: *Provide a brief list of keywords (limit to 20 words).*

Shock Treatment, Burns, Hemorrhage, Closed Loop, Fluids, Pressors, Hypotension

3. ACCOMPLISHMENTS:

- **What were the major goals of the project?**

Year 01: Develop: 1) An extensive set of physiological data of responses to injuries and therapeutics using anesthetized swine animal experiments. 2) New mathematical models suited to the development and validation of closed-loop resuscitation algorithms for hemorrhage, burns, and refractory shock.

Year 02: Deliver: 1) Validation data will be provided by a series of animal studies 2) Quantitative assessments of the developed mathematical models of hemorrhage, burn shock and refractory shock running in silico closed loop models.

- **What was accomplished under these goals?**

1) major activities;

We performed animal studies of hemorrhages and fluid therapy to generate new data on shock and resuscitation. We also used historic data from our lab on hemorrhage and burn injury and resuscitation studies. These datasets allowed our mathematical modelers to enhance our existing models of fluid therapy of shock and develop new models.

2) specific objectives;

Develop a dataset of animal studies of shock and resuscitation.

Develop mathematical models of fluid therapy of hemorrhage and burn shock and vasopressor drug therapy.

3) significant results or key outcomes.

A mathematical Burn Model is now completed, see 3a. Good progress was made in our hemorrhage model, see 3b, which is still undergoing some refinements.

Physiological Dataset

Animal preparation and measured variables. Anesthetized (Isoflurane) swine were splenectomized and instrumented with catheters and sensors in order to monitor blood pressure (arterial, central venous, and pulmonary), heart rate, cardiac output, urinary output and pulse oximetry. Blood samples were taken every 5 to 15 minutes for hematocrit determinations to assess volume expansion with bolus therapy. In addition, blood gases were measured during each experimental period.

Protocol. After surgery and stabilization, there was a one hour baseline period, then each protocol had four to seven periods of shock and resuscitation. Multiple protocols were then performed. The exact protocols were discussed and established before each experiment (video-teleconference call) by the entire group. The goal was to provide the modelers with shock and fluid challenges and their time points needed to develop and test the model. Typically, we performed 1-2 hemorrhage periods, in which blood was removed until mean arterial pressure was equal to a predetermined set target, e.g. 40 mmHg, and held at that pressure by additional bleeding or stopped, hemorrhage data was collected was one hour. Each protocol had and 2 to 4 boluses equal to 200-mL to 500 mL per 80m Kg per 80 kg. This provided typical adult human sized boluses. We used 5% albumin for bolus fluids; 5% albumin has the volume expanding effects of plasma or whole blood. We studied rapid bolus and slow boluses.

Data Handling. We have physiological data from 14 swine studies of hemorrhage and resuscitation. Data was manually recorded every 5 into 10 minutes. Shorter sampling times were performed during and just after bolus therapy. Data was transcribed to Excel. We also have high resolution hemodynamic data collected at 1,000 Hz from the vital signs monitor.

Representative data is shown in the below modelling figures.

3a. Burn Mathematical Model

3.1. Model Description

Burn injury is a life-threatening trauma insult that has been responsible for about 10% of combat casualties in recent conflicts. The definite initial therapy is fluid resuscitation titrated to urinary output (UO). The goal of this effort is to propose a physiological model to represent the macroscopic responses of the cardiovascular system to both burn injury and burn resuscitation. In this report, one such model we developed is presented. The model includes three main components: (a) volume kinetics to describe the changes in fluid volume and protein concentration in the vasculature and tissues, (b) renal function to describe the changes in UO, and (c) burn-induced perturbations in volume kinetics.

The volume kinetics component is the backbone of the model. It consists of three compartments: plasma, burnt tissue, and intact tissue, where each is assumed to contain water and albumin. The water and protein balance between these three compartments and the homeostasis therein are maintained by flows formed by the capillary filtration, lymph return, gain (fluid infusion and fluid loss (UO, evaporation), and exudation) (Fig. 1).

The capillary filtration of water and protein depends on the capillary pore size as well as the hydrostatic and colloid oncotic pressures in each compartment that are dictated by the well-known Starling and coupled diffusion-convection equations. The lymph return depends only on the hydrostatic pressure in each compartment. After burn injury, the capillary pore size, the hydrostatic pressure in the burn tissue, and its protein content change. All these perturbations lead to a drastic increase in the amount of fluid and protein filtered from plasma to the burnt and intact tissues. Hence, the plasma diminishes both in its water and in its protein content, while both burnt and intact tissues develop edema.

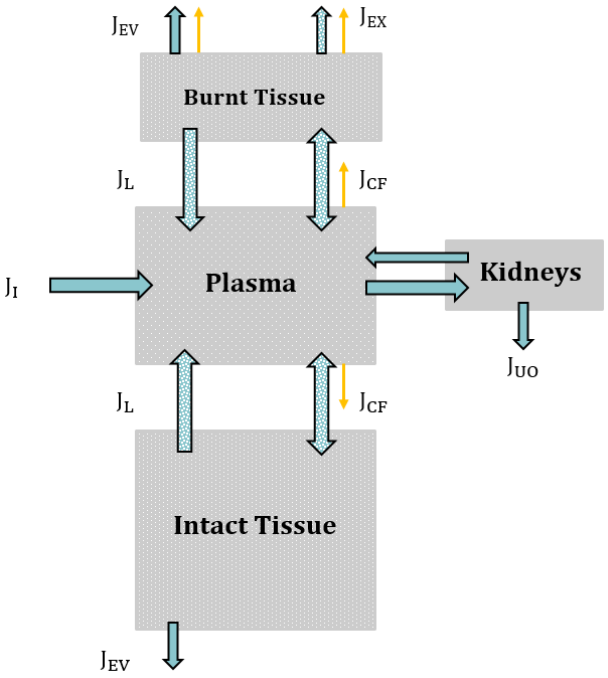

Fig. 5 Schematic of the model, where J: flow, EV: evaporation, EX: exudation, L: lymph, CF: capillary filtration, I: infusion and UO: urinary output. The blue arrows show water flow, and the white dots indicate protein transportation with the flow. The yellow arrows show increase in the shown direction for the corresponding variable directly as a result of burn injury.

The renal function is one of the pivotal fluid regulatory mechanisms in the body. The kidney helps plasma retain its water content by reducing urinary output. Its regulatory mechanisms include the tubule-glomerular feedback and the antidiuretic hormone function, both are triggered by the changes in plasma fluid and protein content.

After writing the appropriate equations for each sub-model and connecting the components, an overall model is constructed, which can potentially represent the macroscopic cardiovascular responses to burns and fluid resuscitation. In this model, n_P= 21 tunable parameters are present, which can be calibrated to capture the characteristics of a subject from measurement data.

3.2. Model Evaluation

The mathematical model above was extensively validated by comparing its predictions to the available experimental data and to literature. The first set of data was collected from 16 sheep with 40% burn injury and included crystalloid infusion rate, urinary output (UO), hematocrit (HCT; which was used to estimate plasma volume (PV)), lymph flow in burnt and intact tissues, and albumin concentrations in PV, burnt tissue, and intact tissues. The mathematical model was nonlinear and complex, involving 24 tunable parameters, which was deemed many relative to the experimental data. Hence, we first examined the feasibility of faithfully fitting the mathematical model to the experimental data using a population-average mathematical model (which was derived by fitting the mathematical model to the experimental data of all 16 sheep) as ground truth. This idealized in silico trial in conjunction with parametric sensitivity analysis showed that the mathematical model

could be fitted well to the experimental data (meaning that (i) the predictions of the mathematical model fitted the ground truth perfectly and (ii) the parameter estimates converged to their ground truth values) when only 11 most sensitive parameters therein were estimated by numerical optimization while the remaining 13 relatively insensitive parameters were fixed at their nominal (i.e., population-average) values. Applying the same scheme to the experimental data on an individual basis resulted in remarkable performance in replicating PV, UO, lymph flow, and albumin concentration in the sheep (Table 1 and Figure 1).

Table 1: Normalized mean absolute error (NMAE; reported in median (IQR)), PV: plasma volume. UO: urinary output. P: plasma. BT: burnt tissues. IT: intact tissues. N indicated the number of subjects for which the measurements were available

	PV [ml] (N=16)	UO [ml/h] (N=16)	Lymphatic Flow [ml/h]		Albumin Concentration [g/l]		
			BT (N=6)	IT (N=7)	P (N=4)	BT (N=2)	IT (N=2)
NMAE [%]	16 (3)	17 (3)	17 (7)	17 (6)	19 (10)	7 (6)	17 (11)

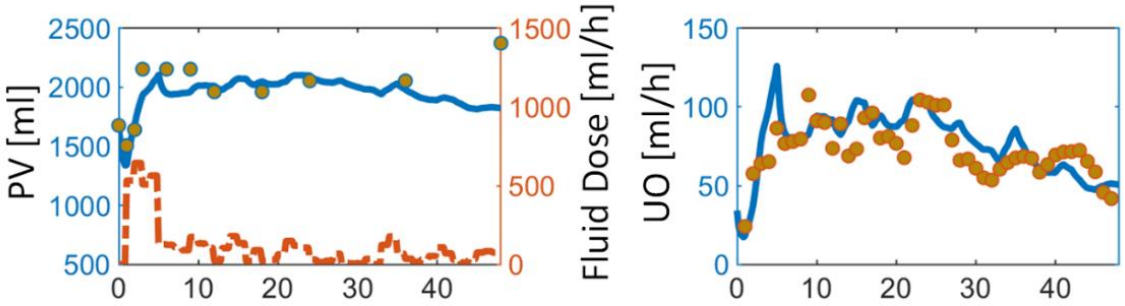

Figure 1: Measured versus model-predicted plasma volume (PV) and urinary output (UO) responses of a 40kg sheep subject to 40% burn. Circles: measured responses. Solid lines: model-predicted responses. Dashed lines: measured fluid dose.

The second set of data included 156 humans (116 training set, 40 test set) with demographics, infusion rate, and UO data. Repeating the same in silico population-average model-based analysis with the human data, we were able to reduce the number of tunable parameters from 24 to 7 sensitive parameters, with only 1% increase in the prediction error. The UO fitting errors for both the training and test set are shown in Table 2.

Table 2: Normalized mean absolute error (NMAE; reported in median (IQR)), PV: plasma volume. UO: urinary output. P: plasma. BT: burnt tissues. IT: intact tissues

	Training Set (N = 116)	Testing Set (N = 40)
UO NMAE [%]	16.2 (6)	15.7 (7)

Figure 2 illustrates the UO prediction for two representative human subjects in the test set. In sum, the mathematical model was able to replicate the UO responses associated with a wide range of burn severity and burn resuscitation regimens. The prediction accuracy was adequate, and the trends of predictions associated with the other physiological variables in the mathematical model were in good agreement with those reported in the literature.

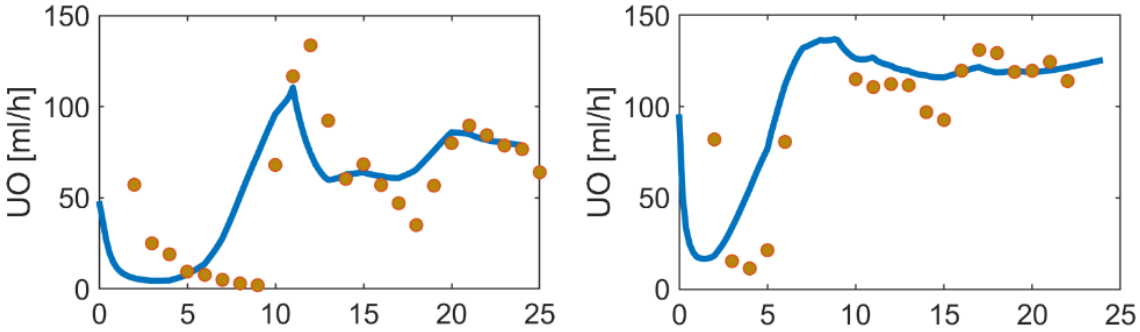

Figure 2: Measured versus model-predicted urinary output (UO) responses in two humans subject to 54% (left) and 30% (right) burn. Circles: measured responses. Solid lines: model-predicted responses.

3b Hemorrhage Mathematical Model

Model Description

1) Main Circulatory System: The circulatory nature of the cardio-vascular system is modeled as a loop, through which the blood flows with rate Q (cardiac output). The heart acts as a pump, which draws blood from the venous compartment and directs it toward the arterial compartment. In addition, a resistance R (systemic vascular resistance) resists the flow of blood through the circulatory system. Furthermore, changes in the volume of each compartment proportionally change the pressure in that compartment. Hemorrhage is modeled as a loss of volume in the circulatory system, while fluid resuscitation is modeled as a volume expansion.

2) Fluid Shift Mechanism: In the absence of perturbations, the volume of blood in the main circulatory system is assumed to be in relative equilibrium with the volume of fluid in the interstitial compartment. A perturbation in blood volume (e.g. hemorrhage or fluid resuscitation) is partially counteracted by a shift of fluid to/from the interstitial compartment. The net rate of fluid shift J_f is thus modeled as the control input of a hypothetical controller that has the goal of regulating total blood volume.

3) Systemic Vascular Resistance Regulation: The resistance denoted by *R* represents the resistance to blood flow that is present throughout the vascular system. The body can change this resistance to some extent through vasoconstriction and vasodilation in order to partially restore a lower-than-normal arterial pressure. In addition, a change in the volume fraction of red blood cells in the blood (*H*) directly affects blood viscosity, which in turn affects *R*. The change in resistance *R* is therefore modeled as a control input that has the goal of regulating arterial pressure, and is also disturbed by changes in *H*.

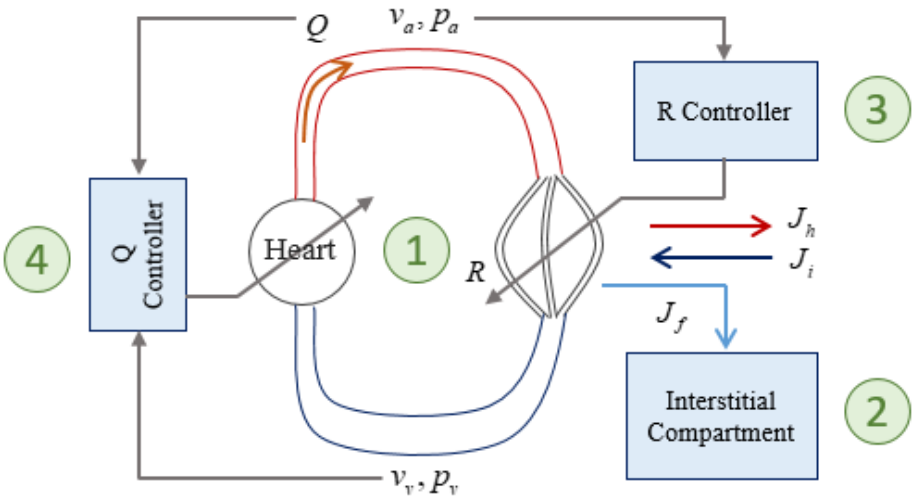

Figure 1: Schematic drawing of the proposed model of cardiovascular responses to fluid perturbation

4) Cardiac Output Regulation: The cardiac output Q can be affected by several important mechanisms: The Frank-Starling mechanism is related to the inherent properties of cardiac muscles, where a higher preload (~proportional to venous pressure) results in a more forceful stroke (and higher stroke volume) in a single beat. The cardiac contractility and heart rate are controlled over time by the autonomic nervous system to maintain a suitable cardiac output Q. Overall, to obtain a minimal representative model of these effects, the cardiac output Q is assumed to be regulated as a controlled variable by a controller that acts through changing a hypothetical control input (which corresponds to both the heart rate and cardiac contractility), and is disturbed by changes in cardiac preload and loss of red blood cells.

In Summary, after writing the appropriate equations for each sub-model and connecting the components, an overall model is constructed, which can potentially represent the macroscopic cardiovascular responses to hemorrhage and fluid resuscitation. In this model, n_p=11 tunable parameters are present, which can be calibrated to capture the characteristics of a subject from measurement data.

3.4. Hemorrhage Model Evaluation Using Existing Datasets

The validity of the mathematical model of hemorrhage and resuscitation in Figure 1 was evaluated using the in-house dataset collected from 23 sheep subject to hemorrhage and resuscitation, which illustrated that the mathematical model could faithfully replicate the experimental dataset. Figure 2 shows a few representative examples of the experimental dataset and mathematical model predictions after fitting.

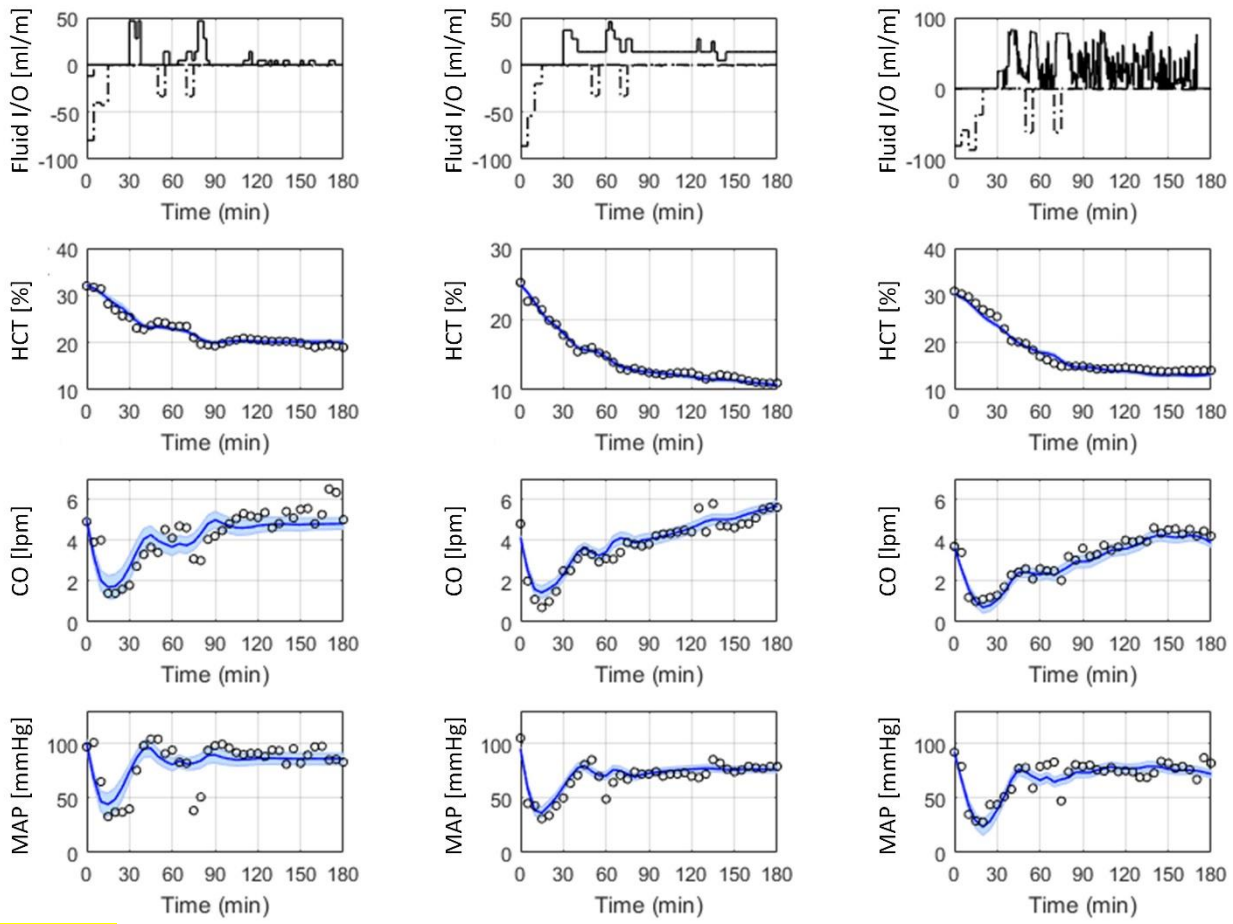

Figure 2: Experimental hematocrit (HCT), cardiac output (CO), and mean arterial pressure (MAP) data and the corresponding predictions by fitted mathematical model of hemorrhage and resuscitation.

3.3. Analysis of FORwARD Hemorrhage Dataset

A data processing pipeline was established to prepare the data to be used to train, modify, and validate the mathematical model of hemorrhage and hemorrhage resuscitation. To date, we have received, processed, and analyzed experimental data associated with 11 animals subject to four different hemorrhage-colloid bolus protocols. Our mathematical model seemed to successfully predict the general trend of cardiac output (CO) and mean arterial pressure (MAP) in most animals. However, it had difficulty in replicating a transient undershooting and rebounding behavior observed in the hematocrit (HCT) measurements (Figure 3).

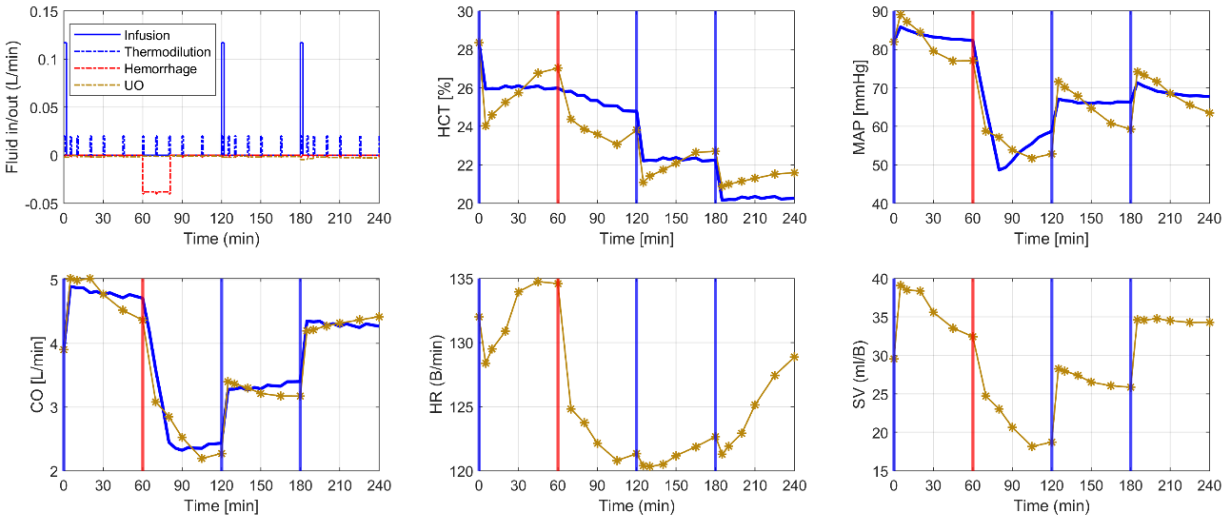

Figure 3: HCT: hematocrit, MAP: mean arterial pressure, CO: cardiac output, HR: heart rate, SV: stroke volume. The starred gold line shows the filtered data, and the solid blue line shows the prediction. In all the plots, the vertical blue line shows the timing of bolus infusion, while the vertical red line shows the timing of hemorrhage insult.

With a closer look at HCT measurements, we detected two common behaviors that were not in agreement with the assumptions and capabilities of the mathematical model. The first behavior is a large dilution of HCT followed by an increase in HCT after approximately 30 minutes. This behavior occurred in 45% of all the hemorrhage insults given to the animals. In contrast, our expectation was that the HCT would monotonously decrease after hemorrhage based on the physiological knowledge: due to RBC loss and a potential fluid shift from the interstitial compartment to the vascular compartment in response to general blood loss. The second behavior is an excessive decrease in HCT after the bolus infusion, usually followed by an increase in HCT until it reaches higher, closer-to-expected values. This behavior happens in about 80% of all the bolus infusions given to the animals. In contrast, our expectation was for the mathematical model to predict a much smaller decline in HCT. The HCT panel in Figure 3 illustrates these behaviors. Another example is shown in Figure 4, where the HCT data was not filtered to clearly illustrate the magnitude of the undershooting/rebounding behaviors.

As these observations were very consistent in our dataset to be deemed as noise, we started to consult the literature to understand potential reasons and mechanisms underlying these behaviors. We had two possibilities in mind. First, that there is a systematic error in measuring the whole-body HCT, i.e. some phenomenon is compromising its estimation. To mention a few, there is a series of studies by Shoemaker et al., introducing a concept related to the delayed-mixing of red blood cells after traumatic hemorrhage and infusion of high-viscosity fluids [1]–[3]. This would mean that after such interventions, a fraction of red blood cells would not circulate as fast, which would result in the underestimation of HCT. This slowly-mixing red blood cells would then gradually mix with the circulation and subsequently bring the HCT up to nominal level. The physiology behind the phenomenon is being more rigorously studied by the study team. But in any case, the observations seem to be consistent with what we are observing in our data.

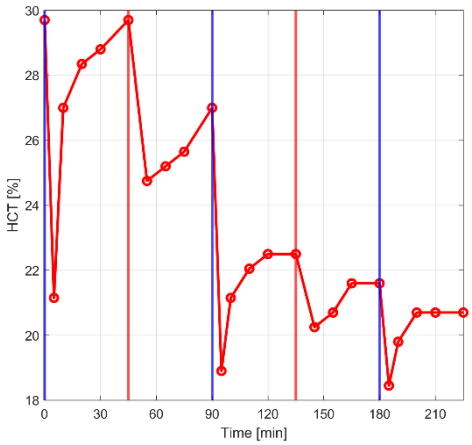

Figure 4: the unfiltered HCT data. The vertical blue line shows the bolus infusion, while the vertical red line shows the beginning of hemorrhage. The HCT goes down remarkably after the bolus infusion and hemorrhage, and then recovers.

It should be noted that, in our data, the measured HCT is the large-vessel HCT but not the very hard-to-measure whole-body HCT. To estimate the whole-body HCT, the measured HCT is multiplied by the ratio of whole-body HCT to the large-vessel HCT, called the f-cell ratio. This ratio is normally equal to around 0.9. However, studies have shown that this ratio transiently increases after hemorrhage and infusion [4]–[6]. The increase in the f-cell ratio after hemorrhage and infusion, has been attributed mainly to the re-distribution of microvascular fluid and the perturbation in the fluid shift between vascular and interstitial compartments. It is worth mentioning that slowly-mixing red blood cells would also lead to an increase in the f-cell ratio. A transiently increased f-cell ratio would at least to some extent explain the HCT undershooting/rebounding behavior in our data, but more data is needed to specify the extent and time of this alteration before being able to translate it into a mathematical model.

Another potential source of perturbation in HCT could be splenectomy, which in case of our animals was performed only 1-2 hours prior to the study. According to Boysen et al. [7], splenectomy can precondition the animals for inflammation and exaggerated responses to hemorrhage, as well as increase the baseline HCT due to the released red blood cells into the circulation immediately before the removal of the spleen. This by itself does not explain the HCT undershooting/rebounding behavior. However, its contribution to the creation of a traumatic state in the animals could lead to other phenomena that more directly affect the red blood cells, such as the slowly mixing RBC's of Shoemaker et al.

Aside from the possibility of systematic errors in whole-body HCT estimation, it could be the case that this excessive dilution and recovery of HCT is due to some transient, two-way fluid shift between the vascular, interstitial, and intracellular compartments. Margarson and Soni [8], in their study on septic and normal human subjects, observed HCT behaviors similar to ours after a fast bolus infusion of albumin 20%. The excessive HCT dilution in their study could be attributed to the high-viscosity fluid drawing water from the interstitial compartment. In our study, the albumin 5% infusion is much less hypertonic,

but could have drawn fluid from the interstitial compartment and further diluted the HCT due to its large amount. A more similar study by Doberneck [9] reported the observation of the same HCT behavior after hemorrhage and attributed it to an increased filtration fraction in kidneys about 30 minutes post-hemorrhage, which would decrease the effective circulating water in the vascular compartment and increase the HCT. This increased filtration fraction post-hemorrhage was also confirmed by Gill and Casper [10]. Finally, a study by Carlson et al. [11] shows that normal blood volume restitution after hemorrhage is impaired when the hemorrhage exceeds some critical level (~>30%). The normal blood volume restitution would lead to a shift from interstitial compartment to the vascular compartment via lymph flow and further diluting the HCT, but the observed impairment in larger hemorrhages compromises this inward fluid shift, and instead, the fluid would shift from the vascular compartment into the interstitial compartment, decreasing plasma volume and increasing HCT, thus explaining the HCT rebounding behavior in some of the animals in our study.

In conclusion, all of these scenarios could be, at least in part, responsible for the commonly observed HCT undershooting/rebounding behavior in our data. While trying to understand the phenomenon deeply and gathering more data, we are focusing on the delayed-mixing RBC concept introduced by Shoemaker et al. due primarily to its ability to explain our observations.

References

[1] W. C. Shoemaker, “Studies on Viscosity Alterations in Shock: I. Effect of High and Low Viscosity Dextrans Upon Plasma and Red Cell Volumes,” *Arch. Surg.*, vol. 87, no. 2, pp. 355–364, Aug. 1963.

[2] F. Suzuki, R. J. Baker, And W. C. Shoemaker, “Red Cell And Plasma Volume Alterations After Hemorrhage And Trauma.,” *Ann. Surg.*, vol. 160, no. 2, pp. 263–274, 1964.

[3] W. C. SHOEMAKER and F. IIDA, “Studies on the equilibration of labeled red cells and T-1824 in hemorrhagic shock.,” *Surg. Gynecol. Obstet.*, vol. 114, pp. 539–44, May 1962.

[4] F. A. Khan, R. Mullins, A. M. Ledgerwood, and C. E. Lucas, “Variability of the f-cell ratio after treatment of traumatic hemorrhagic shock,” *Ann. Med. Surg.*, vol. 35, pp. 176–179, Nov. 2018.

[5] M. Haller, H. Brechtelsbauer, C. Akbulut, W. Fett, J. Briegel, and U. Finsterer, “Isovolemic hemodilution alters the ratio of whole-body to large-vessel hematocrit (F-cell ratio). A prospective, randomized study comparing the volume effects of hydroxyethyl starch 200,000/0.62 and albumin.,” *Infusionsther. Transfusionsmed.*, vol. 22, no. 2, pp. 74–80, Apr. 1995.

[6] H. Hinghofer-Szalkay, “Continuous blood densitometry: Fluid shifts after graded hemorrhage in animals,” *Am. J. Physiol. - Hear. Circ. Physiol.*, vol. 250, no. 3, 1986.

[7] S. R. Boysen, N. A. Caulkett, C. E. Brookfield, A. Warren, and J. M. Pang, “Splenectomy versus sham splenectomy in a swine model of controlled hemorrhagic shock,” *Shock*, vol. 46, no. 4, pp. 439–446, 2016.

[8] M. P Margarson and N. C. Soni, “Changes in serum albumin concentration and

volume expanding effects following a bolus of albumin 20% in septic patients | Elsevier Enhanced Reader," *Br. J. if Anesth.*, vol. 92, no. 6, pp. 821–826, 2004.
[9] R. C. Doberneck and B. Zimmermann, "Early mechanisms of homeostasis after hemorrhage in man," *J. Surg. Res.*, vol. 4, no. 1, pp. 36–42, Jan. 1964.
[10] J. R. Gill and A. G. Casper, "Role of the sympathetic nervous system in the renal response to hemorrhage.," *J. Clin. Invest.*, vol. 48, no. 5, pp. 915–922, 1969.
[11] D. E. Carlson, M. D. Kligman, and D. S. Gann, "Impairment of blood volume restitution after large hemorrhage: A mathematical model," *Am. J. Physiol. - Regul. Integr. Comp. Physiol.*, vol. 270, no. 5 39-5, 1996.

4) Stated goals not met.

Only 14 swine experiments completed due to delays with ACURO delayed approval and Covid-19 UTMB shut down. Vasopressor studies and their models are pending. Overall year 01 modeling tasks are 66% complete with two models done and one pending.

Limited animal studies: We received ACURO approval in November 2019 and with the time periods between ordering, receiving, routine quarantining after arrival, we performed two experiments in the first quarter. Then All UTMB laboratories shut down most of the 4th quarter Apr-Jun 2020 due to Covid-19, but our modelling efforts continued using the data that we had and historic data.

UTMB is now opened at 50%. We are now allowed to move forward, but with social distancing after animal preparation. Once, we were back online our animal supplier was not, so there was a delay in ordering animals. Our animal supplier is now back in business and we received a shipment during the end the last quarter.

- **What opportunities for training and professional development has the project provided?**

Nothing to report

- **How were the results disseminated to communities of interest?**

Results of our research has been distributed in one manuscript, one Proceedings paper and one abstract to the to the Research Community. See publications below.

- **What do you plan to do during the next reporting period to accomplish the goals?**

We will continue to generate physiological datasets using our swine model. We will continue with our animal studies, but at an accelerated pace. We also expect to request a no cost extension to make up for the lost time.

After a few more hemorrhage experiments, we plan to focus on pressor studies using phenylephrine.

We will then start the closed loop treatment studies of hemorrhage, burns and pressors. We will compare the modelling in silico responses versus animal data. After that the mathematical models may be tuned and adjusted for their final format.

4. IMPACT:

- **What was the impact on the development of the principal discipline(s) of the project?**

The mathematical models that we are developing may provide the medical community the means to better assess the safety and efficacy of autonomous care systems. While these models contribute to the general physiological modelling literature, they are designed to provide specific tools for those developing closed loop resuscitation systems.

- **What was the impact on other disciplines?**

Nothing to report

- **What was the impact on technology transfer?**

Nothing to report

- **What was the impact on society beyond science and technology?**

Nothing to report

5. CHANGES/PROBLEMS:

- **Changes in approach and reasons for change**

Because of the less than expected number of animal studies due to late ACURO approval and Covid-19 Pandemic we have also analyzed historic data in addition to our data from our current Forward project**.**

- **Actual or anticipated problems or delays and actions or plans to resolve them**

- **Changes that had a significant impact on expendit**ures.

Because of the delays in hiring some personnel and a delay due to ACURA approval the animal research and our expenditures are behind, we will request a no cost extension for a Year 03 effort.

- **Significant changes in use or care of human subjects, vertebrate animals, biohazards, and/or select agents**

None

- **Significant changes in use or care of human subjects**

Not applicable

- **Significant changes in use or care of vertebrate animals**

Nothing to report

- **Significant changes in use of biohazards and/or select agents**

None used, nothing to report.

6. PRODUCTS: *List any products resulting from the project during the reporting period. If there is nothing to report under a particular item, state "Nothing to Report."*

- **Publications, conference papers, and presentations**

  Peer reviewed Manuscript*.*

  Ghazal ArabiDarrehDor, Ali Tivay, Ramin Bighamian, Chris Meador, George C. Kramer, Jin-Oh Hah and Jose Salinas "Mathematical Model of Volume Kinetics and Renal Function after Burn Injury and Resuscitation", In press, Burns 2020

  Proceedings paper

Ali Tivay, George C. Kramer and Jin-Oh Hahn,. Virtual Patient Generation using Physiological Models through a Compressed Latent Parameterization. Proceedings of the 2020 American Control Conference
Denver, CO, USA, July 1-3, 2020

Abstract-Presentation

Ghazal ArabiDarrehDor, Ali Tivay, Ramin Bighamian, Chris Meador, George C. Kramer,, Jin-Oh Hah and, Jose Salinas. "Development and Evaluation of a Mathematical Model of Volume Kinetics and Renal Function after Burn Injury and Resuscitation ", Published and presented online, Military Health Science Research Symposium (MHSRS), 2020. *

- **Website(s) or other Internet site(s)**

  MHSRS abstracts published

  https://militaryhealthinstitute.org/view-the-2020-mhsrs-accepted-abstracts/

- **Technologies or techniques**

  Nothing to Report

- **Inventions, patent applications, and/or licenses**

  Nothing to Report

- **Other Products**

  Two mathematical models produced, one for burn shock and fluid resuscitation and one for fluid resuscitation of hemorrhagic hypovolemia and fluid therapy.

  One has been published on and the other will be published.

7. PARTICIPANTS & OTHER COLLABORATING ORGANIZATIONS

- **What individuals have worked on the project?**

No Changes from project start.

Investigators Name: George Kramer, PhD
Project Role: PI, UTMB
12 months, from project start

Name: Jin-Oh Hahn, PhD
Project Role: Co-I, University of Maryland
12 months, from project start

Name: Michael Kinsky, MD
Project Role: Co-I, UTMB
No Change
12 months, from project start

Name: Christopher Scully, PhD
Project Role: Co-I, Food & Drug Administration
Researcher ID 0001-8244-0832
12 months, from project start

Name: Ramin Bighamian
Project Role: Co-I, Food & Drug Administration
12 months from project start

Contribution to Project: Blood volume model enhancement to be used for physiologic closed-loop control evaluation. Regulatory perspectives and performed working on planning the data collection methods and analyses for model evaluation. No change in months worked.

Name: Ali Tivay
Project Role: PhD Student, University of Maryland
Researcher ID 0002-2003-1109
Months worked on project: 12 months from project start
Contribution to Project: Parameter estimation and enhanced modeling of cardiovascular responses to hemorrhage and fluid resuscitation. No change in months worked.

Name: Ghazal Arabidarrehdor
Project Role: PhD Student, University of Maryland
Months worked on project: 12 months from project start

Contribution to Project: Blood volume model enhancement to be used for physiologic closed-loop control evaluation. From project start

Name: Randy Salsbury
Project Role: Research Associate II, UTMB
Months worked on project: 12 months from project start
Contribution to Project: Animal surgery and experiments. No change in months worked.

Name: Weihua Cui
Project Role: Research Associate II, UTMB
months worked on project: 6
Contribution to Project: Animal surgery and experiments. New hire Research Associate

- **Has there been a change in the active other support of the PD/PI(s) or senior/key personnel since the last reporting period?**

No changes, Nothing to report.

- **What other organizations were involved as partners?**

Same investigators and their Organizations as at project start.

University of Maryland – Mathematical Modeling engineers

FDA – Regulatory and Clinical Perspective of Modeling

UTMB – Animal studies

8. SPECIAL REPORTING REQUIREMENTS

COLLABORATIVE AWARDS:

None

QUAD CHARTS:

Attached

Mathematical Modeling of Hemodynamics in Trauma-Induced Shock for Closed-Loop Fluid and Drug Resuscitation

Task Title: FORwARD - Autonomous and Unmanned Medical Capability

PI: GC Kramer **Org:** UTMB, Univ. Maryland, FDA

Award Amount: $1,294,591

Specific Aims:

1) Development of Mathematical Models of Trauma-Induced Shock and Resuscitation
2) Quantitative Evaluation of Mathematical Models of Trauma-Induced Shock and Resuscitation
3) Establish Utility of the Mathematical Models by Comparing In Silico and Animal Testing of Closed Loop Resuscitation Algorithms

Approach: Collect animal data of shock and resuscition

We perform animal studies to provide to modelers. We advance closed-loop algorithms for fluid and drug resuscitation for trauma care by developing, validating, and utilizing mathematical models.

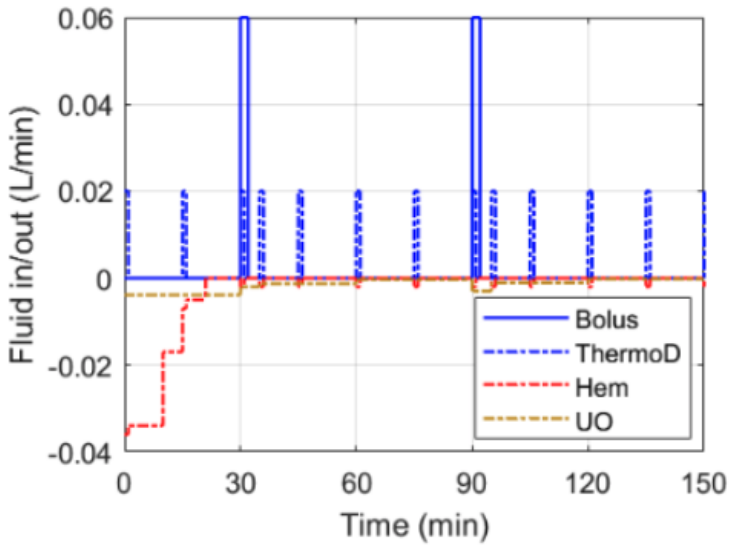

Timeline and Cost

	Aims and Goals	Year 01	Year 02
Aim 1:	Swine Studies Data Generation, n= 32		
Aim 1:	Model Develoment		
Aim 2:	Swine Studies Data Generation, n= 32		
Aim 2:	Model Evaluation		
Aim 3:	In Silico, Closed Loop (CL) vs. Animal CL data		
	Extimated Budget:	$645,635	$648,956

Updated: July 2020

Goals/Milestones

Year 01 Goal – Perform 32 animal studies of dose response (fluids & pressors generating data for model development. Develop mathematical models for hypovolemic hemorrhage, burn injury and refractory shock and their treatments with fluids and phenylephrine.

Year 02 Goals – Perform 32 animal studies to allow evaluation and tuning of developed mathematical models. Compare possible confliction and interplay of two closed-loop therapies, fluids and pressors.

Comments/Challenges: We are behind in our animal schedule due to late ACURO approval and Covid pandemic. We will be requesting a no cost Year 03 extension.

Budget Expenditure to Date: $270,628

Projected Expenditure: from ledger – **$645,635**

9. APPENDICES:

Publications attached

Peer reviewed Manuscript*.*

Ghazal ArabiDarrehDor, Ali Tivay, Ramin Bighamian, Chris Meador, George C. Kramer, Jin-Oh Hah and Jose Salinas "Mathematical Model of Volume Kinetics and Renal Function after Burn Injury and Resuscitation", In press, Burns 2020

Proceedings paper

Ali Tivay, George C. Kramer and Jin-Oh Hahn,. Virtual Patient Generation using Physiological Models through a Compressed Latent Parameterization. Proceedings of the 2020 American Control Conference
Denver, CO, USA, July 1-3, 2020

Abstract-Presentation

Ghazal ArabiDarrehDor, Ali Tivay, Ramin Bighamian, Chris Meador, George C. Kramer,, Jin-Oh Hah and, Jose Salinas. "Development and Evaluation of a Mathematical Model of Volume Kinetics and Renal Function after Burn Injury and Resuscitation ", Published and presented online, Military Health Science Research Symposium (MHSRS), 2020. *

Mathematical Model of Volume Kinetics and Renal Function after Burn Injury and Resuscitation

Ghazal ArabiDarrehDor[1], Ali Tivay[1], Ramin Bighamian[2], Chris Meador[3], George C. Kramer[3,4]
Jin-Oh Hahn[1†], Jose Salinas[5]

[1]: Department of Mechanical Engineering, University of Maryland

[2]: U.S. Food and Drug Administration

[3]: Arcos, Inc.

[4]: Department of Anesthesiology, University of Texas Medical Branch

[5]: U.S. Army Institute of Surgical Research

[†]: Corresponding Author

Disclaimer

This article reflects the views of the author and should not be construed to represent FDA's views or policies.

Abstract

This paper presents a mathematical model of blood volume kinetics and renal function in response to burn injury and resuscitation, which is applicable to the development and non-clinical testing of burn resuscitation protocols and algorithms. Prior mathematical models of burn injury and resuscitation are not ideally suited to such applications due to their limited credibility in predicting blood volume and urinary output observed in wide-ranging burn patients as well as in incorporating contemporary knowledge of burn pathophysiology. Our mathematical model consists of an established multi-compartmental model of blood volume kinetics, a hybrid mechanistic-phenomenological model of renal function, and novel lumped-parameter models of burn-induced perturbations in volume kinetics and renal function equipped with contemporary knowledge on burn-related physiology and pathophysiology. Using the dataset collected from 16 sheep, we showed that our mathematical model can be characterized with physiologically plausible parameter values to accurately predict blood volume kinetic and renal function responses to burn injury and resuscitation on an individual basis against a wide range of pathophysiological variability. Pending validation in humans, our mathematical model may serve as an effective basis for in-depth understanding of complex burn-induced volume kinetic and renal function responses as well as development and non-clinical testing of burn resuscitation protocols and algorithms.

Keywords: Mathematical Model, Burn Injury, Burn Resuscitation, Non-Clinical Testing, Burn Resuscitation Protocols and Algorithms

Introduction

Burn resuscitation is a major critical care challenge. Immediately post burn, a large amount of intravascular fluid and protein is shifted into the interstitial space due to a chain of events initiated by the heat-induced inflammatory response of the body [1], [2]. Subsequent plasma loss in the intravascular space compromises cardiac performance, which may lead to end organ hypo-perfusion, ischemia, and death in

severe burns [3], [4]. In critical care units, this loss is compensated for by fluid replacement therapies to replenish blood volume (BV), guided by available burn resuscitation guidelines [5].

In today's clinical practice, physicians frequently adjust fluid resuscitation regimen to maintain an adequate urinary output (UO) as an indicator of fluid replacement [6]. But, there is a lack of consensus on the optimal burn resuscitation strategy, in terms of the timing, amount, and type of fluids to be administered [7]–[10]. Considering that insufficient and delayed resuscitation may increase the mortality risk of burn patients [11], prior therapy in burn units tended to conservatively over-resuscitate patients with excessive amount of fluids up to twice as much as recommended [12], [13], exposing these patients to an elevated risk of side effects, e.g., pulmonary edema, limb and abdominal syndromes, necrosis, and death [14], [15] (known as fluid creep). Hence, optimizing burn resuscitation regimen may significantly contribute in reconciling the maintenance of organ function and the minimization of adverse complications. Conventional evidence-based approach to such optimization involves rigorous in vivo trials in animals and humans. In recent years, both the U.S. and European regulatory agencies have expressed interest in the use of mathematical models of physiological systems as a powerful non-clinical tool for developing and testing clinical therapies [16]–[19]. Hence, a credible mathematical model capable of predicting patient's physiological responses (including BV and UO) to burn injury and resuscitation has the potential to streamline the development of new optimal burn resuscitation regimen.

Prior work on mathematical modeling of burn injury and resuscitation exists. Arturson et al. [20]–[22] developed a phenomenological model using datasets collected from a small number of burn patients. Roa et al. [23]–[25] developed a hybrid mechanistic-phenomenological model using datasets collected from a number of burn patients. Bert et al. [26]–[30] also developed a hybrid mechanistic-phenomenological model using datasets collected from rats and humans. These models provide very good insights into the complicated physiology and pathophysiology associated with the burn injury and resuscitation. But at the same time, opportunities exist for improving the validity and versatility of existing mathematical models, especially in the context of testing burn resuscitation protocols and algorithms. First, a subset of these mathematical models cannot predict UO [26]–[30]. Such a limitation directly disqualifies a mathematical model in the development and testing of burn resuscitation regimen based on UO feedback. Second, the ability of the existing mathematical models to predict PV and UO was validated in a prohibitively small number of patients [20]–[25] or only at the population level [26]–[30]. In addition, the ability of these mathematical models to predict responses other than PV and UO are not reported in detail. Such lack of validity evidence weakens the credibility of these mathematical models as basis for reproducing PV and UO responses associated with wide-ranging burn patients. Third, a subset of the mathematical models (especially those reported early) [20]–[25] do not incorporate contemporary knowledge of burn-related physiology and pathophysiology, regarding in particular the burn-induced perturbations in blood volume kinetics and renal function, lymphatic flow, and tissue pressure-volume relationships [2], [31]–[33]. Closing these gaps may yield an enhanced mathematical model of burn injury and resuscitation better suited to the development and testing of novel burn resuscitation protocols and algorithms.

This paper presents a mathematical model of blood volume kinetics and renal function in response to burn injury and resuscitation, which is applicable to the development and non-clinical testing of burn resuscitation protocols and algorithms. Our mathematical model consists of an established multi-compartmental model of BV kinetics, a hybrid mechanistic-phenomenological model of renal function, and novel lumped-parameter models of burn-induced perturbations in volume kinetics and renal function equipped with contemporary knowledge on burn-related physiology and pathophysiology. We examined the efficacy of our mathematical model in predicting volume kinetic and renal function responses to burn injury and resuscitation using the dataset collected from 16 sheep.

This paper is organized as follows. Section Materials and Methods presents our mathematical model, experimental dataset, and data analysis details. Section Results presents results, which are discussed in Section Discussion. Section Conclusion concludes the paper with future directions.

Material and Methods

Mathematical Model

Our mathematical model includes mechanisms and components to predict responses to burn injury and resuscitation: (i) volume kinetics to describe water volume and protein concentration in the vasculature and the tissues, (ii) renal function to describe UO response to vascular volume changes, and (iii) burn-induced perturbations in volume kinetics and renal function as a cascade of biochemical, molecular, and mechanical events (Fig. 1). Full details of the mathematical model, including all the equations, are provided in Appendix.

The volume kinetics (VK) was represented by a multi-compartmental model consisting of vasculature, intact tissues, and burnt tissues. It describes the fluid and protein balance in each compartment and homeostasis via capillary filtration and lymphatic flow as well as water gain (e.g., burn resuscitation) and loss (e.g., UO, evaporation, and exudation) (see Section A.1). The renal function was represented by a novel lumped-parameter model we developed in this work (Fig. A1; see Section A.2). It consists of hybrid mechanistic-phenomenological components to describe UO control by the kidneys, including the glomerular filtration rate (GFR) modulated by the Starling forces in response to the change in BV as well as the reabsorption and sodium osmosis modulated by the antidiuretic hormone (ADH). The burn-induced perturbations in VK and renal functions were represented by an array of phenomenological models, which describe local and systemic pathophysiological changes induced by burn injury in the form of time-varying perturbations acting on the parameters and variables in VK and renal function (shown as [a], [b], [c], [d],[e], and [f] in Fig. 1; see Section A.3).

Experimental Data

Experimental dataset used to validate our mathematical model was formed by combining the two datasets collected from two prior work under the approval of local Institutional Animal Care and Use Committee [34], [35]. One dataset was obtained from a study conducted on adult sheep (N=8) with the median weight of 40kg and full-thickness burn injury of 40% total body surface area (TBSA). Burn resuscitation by lactated ringers was initiated 1 hour post burn and continued for 48 hours. Resuscitation was performed to maintain a target UO of 1-2ml/kg/h, which is considered as normal UO in sheep. Key measurements in the dataset used in this work include hourly records of fluid infusion and UO, and more sparse measurements of hematocrit (HCT; N=12 per sheep on the average). The other dataset was obtained from another study conducted on adult sheep (N=8) with the median weight of 50kg and full-thickness burn injury of 30% TBSA. Burn resuscitation by lactated ringers was initiated 2 hours post burn and continued for ≥24 hours, while sheep were monitored for 72 hours. Resuscitation was performed to restore and maintain central venous pressure and pulmonary wedge pressure. Key measurements in the dataset used in this work include fluid infusion, UO, and HCT. In a subset of the sheep, measurements of protein concentrations in plasma, burnt tissue, and intact tissue compartments, as well as fractions of lymphatic flow from burnt and intact skin to vascular compartment at lymph nodes were made. These measurements were also used to validate our mathematical model in this work. Table 1 summarizes the measurements available in our dataset.

We computed PV from HCT using a formula reported in prior work [36], [37] based on the assumption that (i) the baseline BV of sheep is 63.5ml/kg and (ii) no blood loss occurred during the course of burn resuscitation (so that red blood cell volume was preserved).

Table 1: Measurement availability in dataset used for mathematical model validation. N: number of subjects associated with the measurement. PV: plasma volume. UO: urinary output. BT: burnt tissue. IT: intact tissue. Albumin: albumin concentration.

	Fluid Dose	PV	UO	Lymph Flow (BT)	Lymph Flow (IT)	Albumin (Plasma)	Albumin (BT)	Albumin (IT)
N	16	16	16	6	8	5	2	2

Data Analysis

We examined the validity of our mathematical model as follows. First, we categorized the parameters in the mathematical model into subject-invariant and subject-specific parameters. Second, we estimated the values of subject-specific parameters by fitting the mathematical model to the measurements in the dataset while fixing subject-invariant parameters to respective pre-specified values. Third, we examined the validity of the mathematical model by analyzing the goodness of fit and estimated parameter values associated with the mathematical model. Details follow.

First, we categorized the parameters in the mathematical model into subject-invariant and subject-specific parameters. Subject-invariant parameters included (i) those (mostly associated with extensive properties and mechanistic components in the mathematical model) whose values appear consistent in multiple prior literatures (e.g., nominal water volume and albumin content in the vascular and tissue compartments and the hydrostatic pressure in Bowman's capsule), and (ii) those whose values must be selected to produce mechanistically relevant physiological responses (e.g., parameters associated with the tissue compliance model, which must be chosen to yield physically relevant tissue hydrostatic pressure for a range of tissue volumes). The values of these subject-invariant parameters were mostly determined based on the existing literature (see Table A1 for specific literatures we used to determine these values). Subject-specific parameters included (i) those whose values are anticipated to exhibit large inter-subject variability (e.g., burn-induced perturbations and nominal glomerular filtration coefficient), (ii) those whose values have rarely been reported in the existing literature (e.g., capillary elastance and nominal lymphatic flow), and (iii) those associated with phenomenological components in the mathematical model whose values are inherently unknown. After all, a total of 58 parameters were categorized into 34 subject-invariant and 24 subject-specific parameters.

Second, we estimated the values of subject-specific parameters by fitting the mathematical model to the measurements in the dataset while fixing subject-invariant parameters to respective pre-specified values. Considering that the amount of measurements in the dataset may not be sufficient to reliably estimate all the 24 subject-specific parameters, we selected a small subset of sensitive subject-specific parameters and estimated them while fixing the remaining insensitive subject-specific parameters to respective population-average values. First, we determined population-average parameter values by fitting our mathematical model simultaneously to all the measurements in all subjects in the dataset using the pooled approach [38]. Second, we estimated all 24 subject-specific parameters on the individual basis by fitting our mathematical model to the measurements associated with each subject, by employing a regularized fitting that intends to minimize the number of parametric deviations from the population-average values [39], [40]. Those subject-specific parameters exhibiting deviations from population-average values in many sheep were chosen as sensitive subject-specific parameters, which were confirmed via a post-hoc parametric sensitivity analysis. This exercise resulted in 11 sensitive subject-specific parameters that must be estimated on the individual basis (see Appendix A.5). Third, we estimated the 11 sensitive subject-specific parameters on the individual basis by fitting our mathematical model to all the available measurements associated with each subject while fixing the remaining 13 insensitive subject-specific parameters to respective population-average values (and as well, fixing subject-invariant parameters to respective pre-specified values). Details regarding the fitting of the mathematical model is provided in Appendix (see A.5). In sum, we derived 16 subject-specific mathematical models as well as a population-average mathematical model using the dataset.

Third, we examined the validity of the mathematical model by analyzing the goodness of fit and estimated parameter values associated with the mathematical model as follows. First, we examined the ability of our mathematical model to predict PV and UO responses on the individual basis, in terms of normalized mean

absolute error (NMAE), correlation coefficient, and the Bland-Altman statistics between actual PV and UO measurements associated with each sheep in the dataset versus PV and UO predicted by our mathematical model characterized with the corresponding subject-specific parameter values. Second, we examined the ability of our mathematical model to predict physiologically plausible VK and renal function responses by (i) quantitatively analyzing, on the individual basis, NMAE, correlation coefficient, and the Bland-Altman statistics between actual lymphatic flow and albumin concentration associated with (a subset of) each sheep in the dataset (see Table 1) versus lymphatic flows and albumin concentrations predicted by our mathematical model characterized with the corresponding subject-specific parameter values, and also (ii) qualitatively comparing VK and renal function responses predicted by our mathematical model characterized by population-average parameters with contemporary knowledge on burn pathophysiology and findings from recent studies. Third, we examined the physiological plausibility of our mathematical model by comparing the subject-specific and population-average parameter values estimated by fitting the mathematical model to the dataset with known typical values and those reported in the literature.

Results

Table 2 summarizes NMAE, correlation coefficient, and the Bland-Altman statistics (i.e., the limits of agreement) associated with PV, UO, lymphatic flow, and albumin concentration predicted by the mathematical model. Fig. 2 presents representative examples of measured versus model-predicted PV and UO responses of two 40kg sheep subject to 40% burn whose PV was resuscitated (a) beyond the pre-burn level and (b) just to the pre-burn level. Fig. 3 presents VK and renal function responses to burn injury and resuscitation predicted by population-average mathematical model in response to population-average burn resuscitation input.

Table 2: Normalized mean absolute error (NMAE; reported in median (IQR)), correlation coefficient (r), and Bland-Altman limits of agreement (LoA) associated with plasma volume, urinary output, lymphatic flow, and albumin concentration predicted by the mathematical model. PV: plasma volume. UO: urinary output. P: plasma. BT: burnt tissues. IT: intact tissues. LoA: 95% limits of agreement (bias+/-2×SD).

	PV [ml] (N=16)	UO [ml/h] (N=16)	Lymphatic Flow [ml/h]		Albumin Concentration [g/l]		
			BT (N=6)	IT (N=7)	P (N=4)	BT (N=2)	IT (N=2)
NMAE [%]	16 (3)	17 (3)	17 (7)	17 (6)	19 (10)	7 (6)	17 (11)
r	0.82	0.66	0.92	0.91	0.85	0.98	0.85
LoA	50+/-404	-8+/-70	0.2+/-5.8	4+/-56	0.5+/-8.2	-0.07+/-3.7	2.3+/-4.0

Discussion

In the lack of consensus on the optimal burn resuscitation regimen and extreme inter-patient physiological variability in burn-induced responses, a credible mathematical model of burn injury and resuscitation may provide a meaningful basis for development and non-clinical testing of burn resuscitation protocols and algorithms in a wide range of patients. Existing mathematical models are associated with at least one of the following limitations: they are (i) not capable of predicting physiological responses essential in measuring the severity of burn injury and the effectiveness of resuscitation (including PV and UO), (ii) not rigorously validated to demonstrate the ability to capture formidable inter-patient variability in burn- and resuscitation-induced responses, and (iii) often equipped with obsolete knowledge of burn pathophysiology. Our goal was to develop a mathematical model of burn injury and resuscitation ideally suited to in-depth understanding of complex burn-induced VK and renal responses as well as development and non-clinical testing of burn resuscitation protocols and algorithms.

Our mathematical model could adequately predict PV and UO responses to burn injury and resuscitation (Table 2 and Fig. 2). In particular, the NMAE associated with our UO prediction was considerably smaller than a recently reported black-box model [41] (30+/-6%) while the underlying UO variability was comparable (44% (our dataset) versus 38% [41] in terms of the coefficient of variation (CoV)). In addition, the level of prediction accuracy was reasonably consistent across subjects (3% in terms of IQR of NMAE for both PV and UO). Further scrutinizing UO prediction, there was 89% agreement between measured and predicted UO in terms of residing in the same range (<0.5ml/h/kg, 0.5-1.0ml/h/kg, and >1.0ml/h/kg) on the average. This is an encouraging performance given that contemporary burn resuscitation protocols adjust resuscitation dose based on UO range rather than its value. All in all, an important related implication is that our mathematical model may be able to capture inter-patient variability in burn-related pathophysiology. In fact, when characterized with individual-specific parameters, our mathematical model could reproduce largely distinct burn- and resuscitation-induced PV and UO responses of apparently similar sheep. For example, Fig. 2 suggests that our mathematical model predicts PV and UO responses associated with two similar sheep of 40kg weight subject to the same 40% burn, but subject to largely distinct initial reduction in PV (approximately 300ml versus 500ml) and its subsequent recovery (200ml versus 1ml above initial PV level). Considering that VK (especially PV) and renal function (especially UO) are direct and surrogate measures of burn resuscitation, respectively, our mathematical model may be adequate for the intended context of use: development and testing of burn resuscitation protocols and algorithms.

In addition to PV and UO, our mathematical model could also predict various VK and renal responses to burn injury and resuscitation not readily accessible via routine clinical measurements in a physiologically plausible fashion. First, VK responses including protein concentrations and lymphatic flows predicted by our mathematical model exhibited adequate agreement with experimental measurements (Table 2). Second, all the VK and renal function responses predicted by our mathematical model exhibited behaviors qualitatively consistent with contemporary knowledge on burn pathophysiology and findings from recent studies in both individual and population-average senses. Fig. 3 presents responses predicted by the population-average mathematical model. To mention a few, the model predicted that (i) PV and UO showed an anticipated trend of initial decline upon the onset the burn injury and subsequent recovery with resuscitation and also with the return of resuscitation fluid leaked into tissues back to vasculature >24 hours post burn (Fig. 3(b), Fig. 3(c), and Fig. 3(e)) [1], [42]; (ii) burnt tissue volume increased up to twice its initial value and peaked approximately at 10-20 hours post burn (Fig. 3(b)) [9]; (iii) intact tissue volume exhibited the same trend but with smaller degree (up to 30% above its initial value; Fig. 3(b)) [9]; (iv) plasma albumin was transported into burnt and intact tissues due to burn-induced perturbations in albumin reflection and permeability-surface area coefficients (Fig. 3(d) and Fig. 3(k); see [e] in Fig. 1) as a result of burn-induced increase in the capillary pore size that decreased the capillary pore radius ratio in both burnt and intact tissue (Fig. 3(i)) [43]; and (v) GFR increased just hours post burn even before PV was restored [44] (Fig. 3(f)). All in all, its ability to make physiologically plausible predictions of VK and renal function makes our mathematical model suited for gaining sophisticated insights not directly available in routine clinical measurements (e.g., UO). For example, our mathematical model predicts that on the average fluid creep peaks at approximately 10 hours post burn and that more than 50% of the resuscitation fluid in the first 24 hours leaks into tissues to exacerbate edema instead of contributing to hemodynamic recovery, which is in good agreement with the findings in the literature (Fig. 3(b) and Fig. 3(c)) [1], [14]. It also predicted that sodium concentration decreased after burn injury and resuscitation, which is also consistent with the findings in the literature [45] (Fig. 3(h)). Provided that rigorous development and testing of burn resuscitation protocols and algorithms require comprehensive understanding and in-depth scrutiny of complex VK and renal function responses to burn injury and resuscitation, this attribute may confer additional credibility for the intended context of use on our mathematical model.

It is worth noting that our mathematical model could predict adequate PV and UO as well as physiologically plausible VK and renal function responses while characterized with physiologically acceptable parameter values. In fact, the majority of model parameters associated with physiological implications assumed values comparable to typical values and/or those reported in the literature both on the individual and population-average basis (Table 3). Such a physiological acceptability in the model parameter values suggests

physiological plausibility (or perhaps even relevance) of our mathematical model, especially the novel mechanisms and components we developed (e.g., our representations for the renal function and burn-induced VK and renal perturbations). It is also worth noting that our mathematical model embraces a wealth of contemporary knowledge on burn physiology and pathophysiology based on findings in recent literatures, including but not limited to burn-induced systemic increase in capillary pore radius [32] and GFR [44] as well as highly nonlinear tissue compliance characteristics dictated by the glycosaminoglycans (GAG) properties [46]. In fact, many of these new findings were made after the pioneering work by Arturson et al. [20]–[22], Roa et al. [23]–[25], and Bert et al. [26]–[30] was conducted. Hence, they were inevitably not incorporated in the existing mathematical models developed by these pioneering researchers. The physiological and mechanistic plausibility of our mathematical model combined with its incorporation of a range of contemporary knowledge on burn pathophysiology allows our mathematical model to predict PV and UO as well as many VK and renal function responses essential to develop and test burn resuscitation protocols and algorithms against a wide range of pathophysiological variability.

Our work has a number of limitations. First, we (somewhat implicitly) assumed that fluid transfers between VK compartments are isotonic and that VK compartments are in electrolyte balance at all times. These are tenable assumptions in that (i) electrolytes pass capillary walls easily, (ii) they are mixed with water quickly and continuously, and (iii) burn resuscitation fluid considered in this work is isotonic lactated ringers. Hence, we assumed that the primary factor governing the changes in electrolyte concentration in the body is related to the change in sodium concentration due to water reabsorption in collecting ducts in the kidneys (which was considered in our renal function model; see Section A.2). Our mathematical model was able to predict VK and renal function responses reasonably well despite these simplifying assumptions, which suggests that the assumptions may be adequate (or at least may not have had drastic impact on the efficacy of the mathematical model). However, these assumptions may not be valid in case of burn resuscitation with fluid other than lactated ringers. Hence, future work on expanding our mathematical model by removing these assumptions is required. Second, our mathematical model only includes extracellular compartments but not intracellular compartment. As a matter of fact, we initially considered intracellular compartment due to its potential importance to electrolyte balance, but it ended up with adding unnecessary complexity to the mathematical model without any meaningful improvement in the goodness of fit. Regardless, intracellular compartment may need to be incorporated in order to broaden the applicability of our mathematical model beyond lactated ringers. Hence, future work on expanding our mathematical model to include intracellular compartment model of adequate complexity and efficacy may be rewarding. Third, the dataset used in this work was associated with rather uniform injury severity (30%-40% TBSA). Despite a wide range of VK and renal function responses in the dataset (Table 1), the narrow range of injury severity may have prevented us from garnering additional insight into, e.g., the dependence of burn-induced perturbations on the injury severity. Hence, future work is required to investigate the adequacy of our mathematical model (especially its phenomenological models of burn-induced VK and renal function perturbations) under a wide range of burn injury severity, and if needed, to improve the validity and efficacy of our mathematical model against wide-ranging burn injury severity. Fourth, the mathematical model was not validated using extensive and ideal VK and renal function measurements. In particular, PV was derived from hematocrit measurements. Despite its well-known direct relationship to PV, its accuracy is not always perfect and is also impacted by disturbances such as hemolysis. In addition, UO was the only renal function measurement used to validate the mathematical model. We illustrated that our mathematical model, by virtue of mechanistic components therein, can at least predict a large number of VK and renal function variables that are qualitatively adequate (Fig. 3). Yet, future work must scrutinize the validity of our mathematical model using robust measurements of more extensive set of VK and renal function measurements.

Conclusions

We developed a mathematical model of burn injury and resuscitation intended for use in the development and non-clinical testing of burn resuscitation protocols and algorithms. Using the dataset associated with

sheep, we demonstrated the potential of our mathematical model for such context of use: it could predict PV and UO as well as a range of VK and renal function responses to burn injury and resuscitation by virtue of its physiological and mechanistic relevance combined with contemporary knowledge of burn physiology and pathophysiology. In order to establish its efficacy as a powerful non-clinical tool for developing and testing burn resuscitation protocols and algorithms, effort must be invested to validate our mathematical model in real-world burn patients associated with a wide range of physiological variability, injury severity, and resuscitation protocol.

Appendix: Mathematical Model Details

A.1. Volume Kinetics

The VK was represented by a classical multi-compartmental model consisting of vasculature, intact tissues, and burnt tissues. It describes the water and protein balance in these compartments and homeostasis via capillary filtration and lymphatic flow as well as water gain (e.g., burn resuscitation) and loss (e.g., UO, evaporation, and exudation). The water and protein balance in each compartment was formulated based on the mass conservation principle:

$$\frac{d(V_P)}{dt} = -J_{C,BT} - J_{C,IT} + J_{L,BT} + J_{L,IT} + J_F - J_U, \quad (1a)$$

$$\frac{d(V_{BT})}{dt} = J_{C,BT} - J_{L,BT} - J_{EX} - J_{EV,BT}, \quad (1b)$$

$$\frac{d(V_{IT})}{dt} = J_{C,IT} - J_{L,IT} - J_{EV,IT}, \quad (1c)$$

$$\frac{d(A_P)}{dt} = -Q_{C,BT} - Q_{C,IT} + Q_{L,BT} + Q_{L,IT} + Q_F, \quad (2a)$$

$$\frac{d(A_{BT})}{dt} = Q_{C,BT} - Q_{L,BT} - Q_{EX} + Q_{PD}, \quad (2b)$$

$$\frac{d(A_{IT})}{dt} = Q_{C,IT} - Q_{L,IT}, \quad (2c)$$

where V is water volume, A is albumin content, J is water flow, and Q is albumin flow. The subscripts C, L, F, U, EV, EX, and PD denote capillary filtration, lymphatic flow, fluid infusion, UO, evaporation, exudation, and protein influx due to burn-induced denaturation (see A.3), respectively, while the subscripts P, BT, IT denote plasma, burnt tissues, and intact tissues, respectively. Note that we assumed that albumin content represents the protein content similarly to prior work [30], [47].

The capillary filtration was expressed using the Starling equation:

$$J_{C,X} = K_{C,X}[P_C - P_X - \sigma_X(\pi_C - \pi_X)], \quad (3)$$

where $X \in \{BT, IT\}$, P_C and P_X are the capillary and tissue hydrostatic pressures, π_C and π_X are the plasma and tissue colloid oncotic pressures, and $K_{C,X}$ and σ_X are the capillary filtration coefficient and the albumin reflection coefficient associated with burnt ($X = BT$) and intact ($X = IT$) tissues, respectively. The colloid oncotic pressure was expressed as a linear function of albumin concentration [47]:

$$\pi_C = C_O[A]_P, \ \pi_X = C_O[A]_X, \quad (4)$$

where C_O is a constant relating albumin concentration to colloid oncotic pressure, and $[A]_P = \frac{A_P}{V_P}$ and $[A]_X = \frac{A_X}{V_X}$ are the plasma and tissue albumin concentrations, respectively. The lymphatic flow was expressed by a phenomenological model in the form of a sigmoidal curve:

$$J_{L,X} = \frac{\bar{J}_{L,X}}{C_L+(1-C_L)e^{-S_L(P_X-\bar{P}_X)}}, \quad (5)$$

where $\bar{J}_{L,X}$ is the nominal lymphatic flow at the nominal tissue hydrostatic pressure of $\bar{P}_X$, and C_L and S_L are constants representing the maximal degree of increase in the lymphatic flow and the its sensitivity to the change in the tissue hydrostatic pressure. Note that this phenomenological model can reproduce the real-world behavior of the lymphatic flow despite its simplicity: (i) it primarily depends on the tissue hydrostatic pressure [48]; (ii) it is proportional to the tissue hydrostatic pressure but eventually saturates; and (iii) it reduces to zero at very low tissue hydrostatic pressure [49].

The albumin transport across the capillary wall was expressed based on the coupled diffusion-convection equation [47], [50]:

$$Q_{C,X} = J_{C,X}(1-\sigma_X)\left\{\frac{[A]_P-[A]_X e^{-\frac{(1-\sigma_X)J_{C,X}}{PS_X}}}{1-e^{-\frac{(1-\sigma_X)J_{C,X}}{PS_X}}}\right\}, \quad (6)$$

where $X \in \{BT, IT\}$, and PS is the permeability-surface area coefficient. The albumin transport associated with the lymphatic flow was expressed in terms of the lymphatic flow and the albumin concentration in the tissues:

$$Q_{L,X} = J_{L,X}[A]_X. \quad (7)$$

The evaporation flow ($J_{EV,X}$, $X \in \{BT, IT\}$ in Eq. (1b)-(1c)) and the exudation flow (J_{EX} in Eq. (1b) and Q_{EX} in Eq. (2b)) were expressed as phenomenological models based on prior work (see Section A.3). The burn resuscitation (J_F in Eq. (1a) and Q_F in Eq. (2a)) is the input provided to the mathematical model.

The capillary (P_C) and tissue (P_X) hydrostatic pressures in Eq. (3)-(5) were expressed as functions of the corresponding water volumes (V_P and V_X). We assumed a linear phenomenological relationship between P_C and V_P:

$$P_C = \bar{P}_C + E_C(V_P - \bar{V}_P), \quad (8)$$

where $\bar{P}_C$ is the nominal capillary hydrostatic pressure associated with the nominal PV $\bar{V}_P$, and E_C is the capillary elastance. We used a nonlinear mechanistic hydrostatic pressure-volume relationship associated with the interstitial tissues at the microscopic level developed by Øien and Wiig [46], and extended it for use with macroscopic measurements. The original model by Øien and Wiig expresses the tissue hydrostatic pressure as a function of the radius R of the spherical glycosaminoglycans (GAG's) therein:

$$P_X = -\frac{\alpha}{R} + \gamma, \quad (9)$$

where α and γ are constant coefficients representing the impact of electrostatic pressure and tissue tension pressure [46] on P_X and

$$R = R(y_X) = \hat{R}\left[1-(1-\beta)\left(\frac{y_X-\hat{y}}{\check{y}-\hat{y}}\right)\right]^n, \quad (10)$$

where y_X is the half-thickness of the extracellular matrix building block (which is a measure of hydration in the tissue X at the microscopic level), $\hat{y}$ and $\check{y}$ are the maximum and minimum values of y_X, $\hat{R}$ is the maximum value of R, β is the ratio between maximum R and nominal R, and n is an exponent describing the GAG response to hydration [46]. We extended Eq. (9)-(10) to compute P_X from macroscopic rather than microscopic (i.e., y_X) measurement by assuming that y_X is proportional to the water volume in the tissues:

$$y_X = 0.75\left(1 + \bar{W}_X \frac{V_X}{\bar{V}_X}\right), \tag{11}$$

where $\bar{W}_X$ is the nominal hydration level defined as the ratio of the water volume in X and its dry weight [33], and the coefficient 0.75 was derived from the assumptions used in prior work of Øien and Wiig [33].

A.2. Renal Function

The renal function was represented by a novel lumped-parameter, hybrid mechanistic-phenomenological model we developed in this work (Fig. A1). It consists of hybrid mechanistic-phenomenological components to describe UO control by the kidneys, including the glomerular filtration rate (GFR) modulated by the Starling forces in response to the change in BV as well as the reabsorption and sodium osmosis modulated by the antidiuretic hormone (ADH). UO is given by the difference between the GFR (J_{GFR}) and the reabsorption rate (RR; J_{RR}):

$$J_U = J_{GFR} - J_{RR}. \tag{12}$$

A.2.1. Glomerular Filtration

GFR is dictated by the Starling forces:

$$J_{GFR} = K_G[P_G - P_B - \sigma_G(\pi_G - \pi_B)] \approx K_G[P_G - P_B - \pi_G], \tag{13}$$

where P_G and P_B are the hydrostatic pressures associated with the glomerular capillaries and the Bowman's capsules, π_G and π_B are the colloid oncotic pressures associated with the glomerular capillaries and the Bowman's capsules, K_G is the glomerular filtration coefficient, and σ_G is the glomerular albumin reflection coefficient. Noting that the membranes in the glomerular capillaries do not allow the passage of albumin, we assumed $\sigma_G = 1$ and $\pi_B = 0$ in Eq. (13).

P_G depends on the renal plasma flow (RPF), a fraction of CO, which is perturbed by the fluctuations in PV but is also regulated by the tubulo-glomerular feedback (TGF) [51]. Assuming that CO is proportional to PV:

$$J_{RPF} = \bar{J}_{RPF} \frac{V_P}{\bar{V}_P}, \tag{14}$$

where J_{RPF} is RPF, and $\bar{J}_{RPF}$ is its nominal value corresponding to the nominal PV $\bar{V}_P$. The perturbations in J_{RPF} due to the fluctuations in PV induced by burn injury and resuscitation are strictly compensated for with the modulation of the renal capillary resistance (called the glomerular resistance [52]) controlled by TGF. We expressed TGF as simple phenomenological dynamic modulation of a hypothetical glomerular resistance R_G:

$$\tau_{TGF} \frac{d\Delta R_G}{dt} = -\Delta R_G + \frac{K_{TGF}}{\bar{J}_{GFR}}(J_{GFR} - \bar{J}_{GFR}), \tag{15}$$

where $\Delta R_G = R_G - \bar{R}_G$ is the modulation of R_G from its nominal value $\bar{R}_G$ enforced by TGF, τ_{TGF} and K_{TGF} are the time constant and the sensitivity associated with TGF, and $\bar{J}_{GFR}$ is the nominal value of GFR. Noting that P_G is proportional to RPF and inversely proportional to R_G (since an increase in R_G results in a decrease in RPF), we expressed P_G as a simple phenomenological function of J_{RPF} and R_G:

$$P_G = \lambda_G \frac{J_{RPF}}{R_G}, \tag{16}$$

where λ_G is a constant coefficient representing the sensitivity of P_G to J_{RPF} and R_G.

We assumed that P_B is constant. Indeed, P_B hardly varies except in rare cases, e.g., when the urinary tract is obstructed [53].

We expressed π_G as a function of π_C (see Eq. (3)) based on the idealistic assumption that albumin content is conserved in the renal capillaries and in the glomerular capillaries:

$$[A]_C J_{RPF} = [A]_G (J_{RPF} - J_{GFR}) \rightarrow [A]_G = \frac{J_{RPF}}{J_{RPF} - J_{GFR}} [A]_C = \frac{1}{1-\varepsilon_{GFR}} [A]_C, \quad (17)$$

where $[A]_G$ is the glomerular albumin concentration and $\varepsilon_{GFR} = \frac{J_{GFR}}{J_{RPF}}$ is the filtration fraction [54]. Hence, based on the assumption that $C_{O,G} = C_O$, i.e., the relationship between albumin concentration and colloid oncotic pressure is the same in the renal capillaries and in the glomerular capillaries, π_G can be expressed by the following for small ε_{GFR}:

$$\pi_G = \frac{1}{1-\varepsilon_{GFR}} \pi_C \approx (1 + \varepsilon_{GFR}) \pi_C. \quad (18)$$

Plugging Eq. (16) and Eq. (18) into Eq. (13) yields the following expression for GFR:

$$J_{GFR} \approx \frac{K_G J_{RPF}}{J_{RPF} + K_G \pi_C} \left[\lambda \frac{J_{RPF}}{R_G} - P_B - \pi_C \right]. \quad (19)$$

Note that GFR is now expressed in terms of PV (J_{RPF}; see Eq. (14)) and plasma albumin content (π_C; see Eq. (4)). Hence, our hybrid mechanistic-phenomenological model of GFR allows us to represent GFR using macroscopic VK.

A.2.2. Reabsorption

RR (J_{RR}) is dictated by the modulation of glomerulotubular balance (GT; $J_{RR,GT}$) and ADH ($J_{RR,ADH}$):

$$J_{RR} = J_{RR,GT} + J_{RR,ADH}. \quad (20)$$

GT modulates the proximal tubules so that approximately 20% of GFR reaches the collecting ducts ($J_{RR,GT} \approx 0.8 J_{GFR}$) [55], [56]. The ADH content is modulated by baroreceptor (due to changes in BV) and osmoreceptor (due to changes in the sodium concentration ([Na^+]) in the blood) to control RR at the collecting ducts [54], [57]. We expressed the dynamics of the ADH content by the following phenomenological model:

$$\frac{d(ADH)}{dt} = K_{ADH} e^{\left(-\lambda_{V_P} \Delta V_P + \lambda_{[Na^+]} \Delta [Na^+]\right)} - 0.27 K_{ADH} [ADH] \frac{J_{GFR}}{\bar{J}_{GFR}} - 0.73 K_{ADH} [ADH] \frac{V_P}{\bar{V}_P}, \quad (21)$$

where ADH is the ADH content in the extracellular fluid, K_{ADH} is the nominal ADH secretion rate, λ_{V_P} and $\lambda_{[Na^+]}$ are positive constant coefficients representing the sensitivity of ADH secretion on the changes in PV and [Na^+], and $[ADH]$ is ADH concentration in the extracellular fluid:

$$[ADH] = \frac{ADH}{V_P + V_{BT} + V_{IT}}. \quad (22)$$

Eq. (20) indicates that ADH secretion increases if PV decreases and/or [Na^+] increases [54]. The coefficients 0.27 and 0.73 come from the notion that ADH is excreted in the kidneys (27%; proportional to GFR [58]) and the liver (73%; proportional to hepatic blood flow, and therefore, approximately to PV [59]). ADH modulates the reabsorption fraction (RF) $\varepsilon_{RR} = \frac{J_{RR,ADH}}{J_{GFR} - J_{RR,GT}}$ to control RR at the collecting ducts. We adopted the Michaelis-Menten equation to express the relationship between $[ADH]$ and the ε_{RR} [57]:

$$\varepsilon_{RR} = K_{RR} \frac{[ADH]}{[ADH]_{50} + [ADH]}, \quad (23)$$

where K_{RR} is the maximum RF, and $[ADH]_{50}$ is the ADH concentration corresponding to $\varepsilon_{RR} = \frac{1}{2} K_{RR}$.

We computed $[Na^+]$ in Eq. (21) based on the idealistic assumption that sodium content is conserved in the body (including the collecting ducts) after burn injury and resuscitation:

$$[Na^+] = \frac{\bar{J}_{RR,ADH}}{J_{RR,ADH}} \overline{[Na^+]}, \tag{24}$$

where $\overline{[Na^+]}$ is the nominal sodium concentration corresponding to the nominal RR $\bar{J}_{RR,ADH}$. That the change in $[Na^+]$ primarily depends on $J_{RR,ADH}$ may be justified to an extent because $J_{RR,ADH}$ consists of pure water diluting the plasma [57].

Substituting Eq. (19), Eq. (20), and Eq. (23) along with $J_{RR,GT} \approx 0.8 J_{GFR}$ into Eq. (12) yields the following expression for UO:

$$J_U = J_{GFR} - J_{RR} = J_{GFR} - J_{RR,GT} - J_{RR,ADH} \approx 0.2 \frac{K_G J_{RPF}(V_P)}{J_{RPF} + K_G \pi_C} \left[\lambda \frac{J_{RPF}(V_P)}{R_G} - P_B - \pi_C\right](1 - \varepsilon_{RR}). \tag{25}$$

Note that UO is now expressed in terms of PV (J_{RPF}; see Eq. (14)) and plasma albumin content (π_C; see Eq. (4)), and ADH concentration. Hence, our hybrid mechanistic-phenomenological model of UO allows us to represent UO using macroscopic VK and ADH dynamics.

A.3. Burn-Induced Pathophysiology in Volume Kinetics and Renal Function

The burn-induced pathophysiological perturbations in VK and renal functions were represented by an array of phenomenological models, which describe local and systemic pathophysiological changes induced by burn injury in the form of time-varying perturbations acting on the parameters and variables associated with VK and renal function. Local perturbations, restricted to burnt tissues, include: (i) destruction of capillaries in burnt tissues [2], (ii) denaturation of protein in burnt tissues [31], [43], [60], (iii) transient negative hydrostatic pressure in burnt tissues [60], [61], and (iv) dermal fluid loss [62], [63]. Systemic perturbations include: (i) time-varying changes in capillary filtration and albumin transport [32] and (ii) vasodilation [64].

We devised a universal function, $\phi(t)$, to represent the time-varying perturbations in all the VK and renal function parameters and variables:

$$\phi\left(M_W, \lambda_{1,W}, \lambda_{2,W}, t\right) = M_W\left(e^{-\lambda_{1,W}t} - e^{-\lambda_{2,W}t}\right), \tag{26}$$

where M_W is the maximum perturbation (occurring after the onset of burn injury), $\lambda_{1,W}$ and $\lambda_{2,W}$ are the slow time constant and fast time constant associated with the decay of the perturbation, all corresponding to a specific perturbation W. The parameter μ denotes the ratio of $\lambda_{2,W}$ to $\lambda_{1,W}$. We used Eq. (26) to express systemic perturbations as well as transient negative hydrostatic pressure in burnt tissues: $W \in \{\alpha_{BT}, \alpha_{IT}, P_C, P_{BT}\}$, where α_{BT} and α_{IT} are pore ratios associated with burnt and intact tissues (see below for details).

A.3.1. Local Pathophysiology

We expressed the destruction of capillaries in burnt tissues as a decrease in the capillary filtration coefficient $K_{C,BT}$ and permeability surface area coefficient PS_{BT} by a factor of k_{PD_X} (see Eq. (32)) [2]. We expressed the denaturation of protein as a protein influx Q_{PD} into burnt tissues [31], [43], [60] (see Eq. 2b):

$$Q_{PD} = \hat{Q}_{PD} e^{-\lambda_{PD} t}, \tag{27}$$

where $\hat{Q}_{PD}$ is the protein influx immediately post burn, decaying with a time constant of λ_{PD}. We expressed the transient negative hydrostatic pressure in burnt tissues using $\phi(t)$ in Eq. (26) as follows:

$$\Delta P_{BT}(t) = -\phi\left(M_{P_{BT}}, \lambda_{1,P_{BT}}, \lambda_{2,P_{BT}}, t\right), \tag{28}$$

where $\Delta P_{BT}(t)$ is the burn-induced perturbation in the hydrostatic pressure in burnt tissues. The overall hydrostatic pressure in burnt tissues is computed by combining Eq. (9) and Eq. (28):

$$P_{BT}(t) = -\frac{\alpha}{R(y_{BT})} + \gamma + \Delta P_{BT} = -\frac{\alpha}{R(y_{BT})} + \gamma - \phi\left(M_{P_{BT}}, \lambda_{1,P_{BT}}, \lambda_{2,P_{BT}}, t\right). \quad (29)$$

We used phenomenological models of evaporation and exudation reported in prior work [65], [66]:

$$J_{EV,BT} = \begin{cases} K_{1,EV}\varepsilon_B S_B e^{\lambda_{1,EV}t}, & t < 6\ hr \\ K_{2,EV}\varepsilon_B S_B e^{\lambda_{2,EV}t}, & t > 6\ hr \end{cases}, \quad (30a)$$

$$J_{EV,IT} = K_{1,EV}\,(1-\varepsilon_B)S_B, \quad (30b)$$

$$J_{EX} = K_{EX}\varepsilon_B S_B e^{\lambda_{EX}t}, \quad (31a)$$

$$Q_{EX} = J_{EX}\eta_{EX}[A]_{BT}, \quad (31b)$$

where $K_{1,EV} > 0$, $K_{2,EV} > 0$ and $K_{EX} > 0$ are constant coefficients, and $\lambda_{2,EV} > 0$, $\lambda_{2,EV} < 0$ and $\lambda_{EX} < 0$ are time constants, ε_B is the fraction of body surface subject to burn, S_B is TBSA, and η_{EX} is the ratio between the albumin concentration in the exudate and the albumin concentration in the burnt tissues [30].

A.3.2. Systemic Pathophysiology

We expressed the systemic impact of burn injury as time-varying changes in the capillary filtration, albumin reflection, and permeability-surface area coefficients (representing perturbations in capillary filtration and albumin transport) as well as capillary hydrostatic pressure (representing perturbation in vasodilation). By capitalizing on the pore theory of trans-capillary exchange [67], [68], we expressed the capillary filtration, albumin reflection, and permeability-surface area coefficients associated with burnt and intact tissues as functions of the pore radius ratios α_X, $X \in \{BT, IT\}$, defined as the ratio between the albumin radius and capillary pore radius:

$$K_{C,X} = \overline{K}_{C,X} k_{PD,X} \frac{\bar{\alpha}_X^4}{\alpha_X^4}, \quad (32a)$$

$$\sigma_X = 1 - (1-\alpha_X)^2, \quad (32b)$$

$$PS_X = \overline{PS}_X k_{PD,X} \frac{\bar{\alpha}_X^2(1-\alpha_X^2)}{(1-\bar{\alpha}_X^2)\alpha_X^2}, \quad (32c)$$

where $\overline{K}_{C,X}$, $\overline{PS}_X$, and $\bar{\alpha}_X$ are the nominal values of $K_{C,X}$, PS_X, and α_X, adjusted for the water fraction in burnt and intact tissues, weight, and capillary recruitment [30]:

$$\overline{K}_{C,BT} = \overline{K}_C \varepsilon_B r_{FV} \eta_{CR},\ \overline{K}_{C,IT} = \overline{K}_C(1-\varepsilon_B r_{FV})\eta_{CR}, \quad (33a)$$

$$\overline{PS}_{BT} = \overline{PS}\varepsilon_B r_{FV}\eta_{CR},\ \overline{PS}_{IT} = \overline{PS}(1-\varepsilon_B r_{FV})\eta_{CR}, \quad (33b)$$

where $\overline{K}_C$ and $\overline{PS}$ are nominal capillary filtration and permeability surface area coefficients in the absence of burn injury, $\eta_{CR} = \left(2\frac{V_P}{\bar{V}_P} - 1\right)$, and r_{FV} is the fluid volume ratio between the skin and the total interstitial compartment [30].

Note that $k_{PD} = 1$ if $X = IT$, because capillary destruction does not occur in intact tissues. We expressed the burn-induced changes in these coefficients by formalizing the burn-induced changes in the capillary pore radius ratios using Eq. (26):

$$\alpha_X(t) = \bar{\alpha}_X - \phi(M_{\alpha_X}, \lambda_{1,\alpha_X}, \lambda_{2,\alpha_X}, t). \quad (34)$$

We likewise expressed the burn-induced change in capillary hydrostatic pressure [64] using Eq. (26):

$$\Delta P_C(t) = \phi(M_{P_C}, \lambda_{1,P_C}, \lambda_{2,P_C}, t). \quad (35)$$

The overall capillary hydrostatic pressure is computed by combining Eq. (8) and Eq. (35):

$$P_C = \bar{P}_C + E_C(V_P - \bar{V}_P) + \Delta P_C(t) = \bar{P}_C + E_C(V_P - \bar{V}_P) + \phi(M_{P_C}, \lambda_{1,P_C}, \lambda_{2,P_C}, t). \quad (36)$$

A.4. Model Parameters: Nomenclature, Definitions and Values

Table A1: Mathematical model parameters: definitions, categories (I/S), and values. I: subject-invariant parameters. S: subject-specific parameters. The vales are given as mean, median (IQR), or mean+/-SD.

Symbol	Definition	I/S	Value (Model)	Value (Literature)
$\overline{BV}$	Nominal blood volume [ml/kg]	I	63.5	63.5 [69]
$\bar{V}_P$	Nominal water volume in plasma [ml/kg]	I	42.8	42 [70]-46 [30]
r_{FV}	Skin fluid volume to total interstitial fluid volume ratio [·]	I	0.28	0.28 [30]
$\bar{V}_{BT}$	Nominal water volume in burnt tissue [ml/kg]	I	$120\varepsilon_B r_{FV}$	$120\varepsilon_B r_{FV}$ [30]
$\bar{V}_{IT}$	Nominal water volume in intact tissue [ml/kg]	I	$120(1-\varepsilon_B r_{FV})$	$120(1-\varepsilon_B r_{FV})$ [30]
$[\bar{A}_P]$	Nominal albumin concentration in plasma [g/ml]	I	0.059	0.059 (0.004) [35]
$[\bar{A}_{BT}]$	Nominal albumin concentration in burnt tissue [g/ml]	I	0.028	0.028 [35]
$[\bar{A}_{IT}]$	Nominal albumin concentration in intact tissue [g/ml]	I	0.028	0.028 [35]
$\bar{A}_P$	Nominal albumin content in plasma [g]	I	$[\bar{A}_P]\bar{V}_P$	-
$\bar{A}_{BT}$	Nominal albumin content in burnt tissue [g]	I	$[\bar{A}_{BT}]\bar{V}_{BT}$	-
$\bar{A}_{IT}$	Nominal albumin content in intact tissue [g]	I	$[\bar{A}_{IT}]\bar{V}_{IT}$	-
$\bar{J}_C$	Nominal capillary filtration [ml/kg·h]	S	1.53 (0.19)	1.72 [29]
C_O	Colloid oncotic pressure constant [mmHg/g·ml]	I	250	250 [35]
$\bar{J}_L$	Nominal total lymphatic flow to plasma [ml/kg·h]	I	1.07 (0.19)	1.08 [30]
$\bar{J}_{L,BT}$	Nominal lymphatic flow from burnt tissue to plasma [ml/kg·h]	I	$\bar{J}_L\varepsilon_B r_{FV}$	$\bar{J}_L\varepsilon_B r_{FV}$ [30]
$\bar{J}_{L,IT}$	Nominal lymphatic flow from intact tissue to plasma [ml/kg·h]	I	$\bar{J}_L(1-\varepsilon_B r_{FV})$	$\bar{J}_L(1-\varepsilon_B r_{FV})$ [30]
C_L	Lymphatic maximal increase coefficient [·]	S	0.29 (0.21)	-
S_L	Lymphatic pressure sensitivity coefficient [1/mmHg]	S	6.44	-
$\bar{P}_C$	Nominal hydrostatic capillary pressure [mmHg]	S	8.0 (0.5)	6.7 (0.8) [71]
E_C	Capillary elastance [mmHg/ml]	S	0.0139	0.0097 [47]
α	Tissue electrostatic pressure coefficient [mmHg]	I	10	10 [46]
γ	Tissue tension pressure coefficient [mmHg]	I	3.75	3.75 [46]
$\hat{y}$	Maximum half-thickness of the extracellular matrix [·]	I	4	4 [46]
$\check{y}$	Minimum half-thickness of the extracellular matrix [·]	I	1	1 [46]
$\hat{R}$	Maximum GAG radius [·]	I	3.5	3.5 [46]
β	Radius threshold ratio [·]	I	0.23	0.23 [46]
n	Hydration response coefficient [·]	I	8	2-8 [46]
$\bar{W}_X$	Nominal hydration level [ml/g]	I	0.66	0.23-0.81 [33], [46]
$\bar{J}_{RPF}$	Nominal renal plasma flow [ml/kg·h]	I	536	536 [72]
τ_{TGF}	Tubuglomerular feedback time constant [1/h]	S	0.35 (0.33)	-
K_{TGF}	Tubuglomerular feedback sensitivity [·]	S	5.75	-
$\bar{R}_G$	Nominal glomerular resistance [mmHg/ml/kg·h]	I	12.34	-
λ_G	Glomerular hydrostatic pressure sensitivity [mmHg^2/(ml/h·kg)^2]	I	1	-
P_B	Hydrostatic pressure in Bowman's capsules [mmHg]	I	18	18 [53]
K_G	Glomerular filtration coefficient [ml/kg·h·mmHg]	S	9.2 (1.2)	9.6-12.0 [73]
K_{ADH}	Nominal ADH secretion rate [pg/kg·h]	I	287	287 [58], [59]
λ_{V_P}	ADH sensitivity to plasma volume change [1/ml]	S	0.0017 (0.0008)	-
$\lambda_{[Na^+]}$	ADH sensitivity to sodium concentration change [l/mEq]	S	0.087	-
K_{RR}	Maximum collecting duct reabsorption fraction [·]	I	0.999	-
$[ADH]_{50}$	ADH concentration corresponding to $\frac{1}{2}K_{RR}$ [pg/ml]	S	0.0628	-
$[\overline{Na^+}]$	Nominal plasma sodium concentration [mEq/l]	I	142	142 [74]
$\bar{J}_{RR,ADH}$	Nominal water reabsorption rate in the collecting ducts [·]	S	0.933 (0.01)	0.97 [55]

$\hat{Q}_{PD}$	Protein influx post burn [g/h]	S	72.98 (53.23)	-
λ_{PD}	Protein influx decay rate [1/h]	S	10	-
$M_{P_{BT}}$	Maximum burnt tissue hydrostatic pressure perturbation [mmHg]	S	38	30 [60]
$\lambda_{1,P_{BT}}$	Burnt tissue hydrostatic pressure perturbation slow decay rate [1/h]	S	5.48	-
μ	The ratio between slow decay rate to fast decay rate [·]	S	356	-
$\lambda_{2,P_{BT}}$	Burnt tissue hydrostatic pressure perturbation fast decay rate [1/h]	I	$8\lambda_{1,P_{BT}}$	-
$K_{1,EV}$	Nominal tissue evaporation rate [ml/h·m^2]	I	18.48	18.48 [66]
$\lambda_{1,EV}$	Evaporation growth rate [1/h]	I	0.073	0.073 [66]
$K_{2,EV}$	Maximum evaporation rate [ml/h·m^2]	I	28.68	28.68 [66]
$\lambda_{2,EV}$	Evaporation decay rate [1/h]	I	-0.0052	-0.0052 [66]
ε_B	Fraction of body surface subject to burn [·]	S	0.3-0.4	dataset
S_B	Total body surface area [m^2]	I	1	1.07+/-0.16 [75]
K_{EX}	Maximum exudation rate [ml/h·m^2]	I	25	25 [65]
λ_{EX}	Exudation decay rate [1/h]	I	-0.0038	-0.0038 [65]
η_{EX}	Exudate to tissue albumin ratio [·]	S	0.69	0.75 [30]
$\bar{\alpha}$	Nominal albumin to capillary pore radius ratio [·]	S	0.82	0.7-0.9 [47]
$k_{PD,BT}$	Capillary destruction fraction [·]	S	0.56	0.50 [28]
$M_{\alpha_{BT}}$	Maximum pore ratio perturbation in burnt tissue [·]	S	0.37	0.30 [31]
$M_{\alpha_{IT}}$	Maximum pore ratio perturbation in intact tissue [·]	S	0.16 (0.11)	0.19 [76]
$\lambda_{1,\alpha}$	Pore ratio slow decay rate [1/h]	S	0.030	0.025 [30]
$\lambda_{2,\alpha}$	Pore ratio fast decay rate [1/h]	I	$\mu\lambda_{1,\alpha}$	-
M_{P_C}	Maximum capillary hydrostatic pressure perturbation [mmHg]	S	19 (12)	23+/-5 [64]
λ_{1,P_C}	Capillary hydrostatic pressure perturbation slow decay rate [1/h]	S	0.54 (0.08)	-
λ_{2,P_C}	Capillary hydrostatic pressure perturbation fast decay rate [1/h]	I	$\mu\lambda_{1,P_C}$	-

A.5. Model Fitting via Numerical Optimization

A.5.1. Classification of Sensitive and Insensitive Subject-Specific Model Parameters

We selected 24 subject-specific parameters in the mathematical model that must be estimated using the datasets, as described in Material and Methods. One dataset [34] had 60 measurements on the average (including 12 PV and 48 UO measurements), while the other dataset [35] had 161 measurements on the average (including 24 PV, 24 UO measurements, 41 lymphatic flow associated with burnt tissues, 50 lymphatic flow associated with intact tissues, 10 plasma albumin concentration, 7 burnt tissue albumin concentration, and 5 intact tissue albumin concentration). The datasets were not deemed too sparse to estimate the subject-specific parameters. But, the amount of measurements in the datasets may not be rich enough to robustly estimate all the 24 subject-specific parameters. Hence, we selected and estimated a subset of sensitive subject-specific parameters on the individual basis while fixing the subject-invariant and insensitive subject-specific parameters to appropriate pre-specified and population-average values. To classify the subject-specific parameters into sensitive and insensitive categories, we examined and compared the degree of inter-individual variability associated with all the subject-specific parameters. First, we determined the population-average parameter values $\bar{\theta}$ by fitting our mathematical model to minimize the cost function in Eq. (37) using the pooled approach [38]:

$$\bar{\theta} = \arg\min_{\theta} \bar{J}(\theta) = \arg\min_{\theta} \sum_{i=1}^{N} \sqrt{\sum_{j=1}^{M_i} \left(\sum_{k=1}^{D_{ij}} \frac{\left| y_{ij}^{d}(t_k) - y_{ij}(t_k,\theta) \right|}{Y_{ij}} \right)^2}, \quad (37)$$

where θ is the vector of subject-specific parameters, N is the number of subjects (=16), M_i is the number of physiological variables measured in the subject i (e.g., M_i=2 if PV and UO were measured), D_{ij} is the number of measurements associated with the physiological variable j in the subject i during the initial 48 hours, $y_{ij}^{d}(t_k)$ is the value of the physiological variable j associated with the subject i measured at time t_k, $y_{ij}(t_k,\theta)$ is the value of the same physiological variable at time t_k predicted by the mathematical model for a given θ, and Y_{ij} is the normalization factor for the physiological variable j associated with the subject i, which is defined as the range of y_{ij}^{d} multiplied by D_{ij} (so that the normalized errors associated with all the

physiological variables have comparable magnitudes across all subjects). Second, we estimated all the 24 subject-specific parameters θ_i associated with the subject i by fitting our mathematical model to all the measurements associated with the subject i to minimize the cost function in Eq. (38), using a regularized fitting that minimizes the number of parametric deviations from the population-average values [39], [40]:

$$\theta_i = \arg\min_{\theta} J_i(\theta) = \arg\min_{\theta} \sqrt{\sum_{j=1}^{M_i}\left(\sum_{k=1}^{D_{ij}} \frac{\left|y_{ij}^d(t_k) - y_{ij}(t_k,\theta)\right|}{Y_{ij}}\right)^2} + \lambda_p \sum_{l=1}^{24}\left|\frac{\theta(l)-\bar{\theta}(l)}{\Theta_l}\right|, \qquad (38)$$

where λ_p is the regularization weight and Θ_l is the normalization factor for the l-th element $\theta(l)$ of θ, which is defined so that all the elements in θ are ranged approximately between 0 and 1 (note that such Θ_l can be estimated by, e.g., solving Eq. (38) with $\lambda_p = 0.05$ and setting Θ_l as the inter-individual variability of the corresponding element $\theta(l)$). Third, using θ_i thus estimated from all the 16 subjects, we computed the average normalized deviation of each element in θ_i. Then, we selected those elements of θ_i associated with deviations thus computed larger than a threshold value as sensitive subject-specific parameters. We set the threshold deviation as 10% based on empiric trial and error, which yielded 12 sensitive subject-specific parameters. Post-hoc parametric sensitivity analysis indicated that the mathematical model was not actually sensitive to one of them, which was thus removed. This exercise yielded a total of 11 sensitive subject-specific parameters (Table A2).

Table A2: Sensitive subject-specific parameters and their average normalized deviations from population-average values.

Parameter	τ_{TGF}	$M_{\alpha_{IT}}$	$\bar{J}_C$	$\bar{J}_{RR,ADH}$	λ_{V_P}	M_{P_C}	λ_{1,P_C}	C_L	$\bar{P}_C$	$\hat{Q}_{PD}$	K_G
Deviation [%]	48.2	18.8	16.9	16.7	16.4	15.3	14	13.2	11.6	11.5	10.3

A.5.2. Model Fitting and Estimation of Subject-Specific Model Parameters

We estimated the 11 sensitive subject-specific parameters selected above on the individual basis by fitting our mathematical model to all the available measurements associated with each subject to minimize the cost function in Eq. (39), while fixing the remaining 13 insensitive subject-specific parameters to respective population-average values ($\bar{\theta}$ in Eq. (37)), and as well, fixing the subject-invariant parameters to respective pre-specified values (see Table A1):

$$\breve{\theta}_i = \arg\min_{\breve{\theta}} \breve{J}_i(\breve{\theta}) = \arg\min_{\breve{\theta}} \sqrt{\sum_{j=1}^{M_i}\left(\sum_{k=1}^{D_{ij}} \frac{\left|y_{ij}^d(t_k) - y_{ij}(t_k,\breve{\theta})\right|}{Y_{ij}}\right)^2} \qquad (39)$$

where $\breve{\theta}$ is the vector of sensitive subject-specific parameters, and $\breve{\theta}_i$ is $\breve{\theta}$ estimated for the subject i.

A.5.3. Numerical Optimization Details

The complexity and nonlinearity associated with our mathematical model strongly suggest the non-convex nature of the numerical optimization problems in Eq. (37)-(39). To derive robust estimates of parameters from our numerical optimization problems, we used multiple initial conditions and tight parameter bounds as follows. First, we used a multi-start gradient descent method in MATLAB ("globalsearch" in conjunction with "fmincon" commands). We empirically selected user-configurable settings (e.g., the number of initial conditions) so that the numerical optimization could yield accurate parameter estimates when simulated measurements associated with the population-average model (i.e., our mathematical model characterized by $\bar{\theta}$ in Eq. (37)) are inputted to Eq. (39). Second, we enforced tight parameter bounds as constraints in solving the numerical optimization problems to effectively guide the solution into a mechanistically plausible parameter space. We carefully specified many of these bounds by leveraging the prior knowledge on the parameter values (see Table A1). It is noted that we intended to also avoid overfitting with these parameter bounds. Since the amount of measurements in our datasets may not be sufficiently large to robustly solve

our numerical optimization problems, mechanistically plausible parameter bounds are expected to benefit in preventing overfitting against measurement noises and errors by keeping the parameter estimates from assuming mechanistically illegitimate values.

All in all, our approach to solve the model fitting problem in Eq. (39) by incorporating (i) a small number of sensitive subject-specific parameters, (ii) multi-start gradient descent, and (iii) parameter bounds appeared to be effective: when Eq. (39) was solved using simulated measurements associated with the population-average model repeatedly, NMAE<0.1% was consistently achieved, and all the 11 sensitive subject-specific parameters had very small errors of <3%.

Funding

This research was supported in part by the U.S. Army SBIR Program [Award No. W81XWH-16-C-0179], the Congressionally Directed Medical Research Programs [Award No. W81XWH-19-1-0322], and the U.S. National Science Foundation CAREER Award [Award No. 1748762].

References

[1] and D. N. H. Kramer, George C., T. Lund, "Pathophysiology of burn shock and burn edema.," in *Total Burn Care*, 2012, pp. 103–13.

[2] C. B. Nielson, N. C. Duethman, J. M. Howard, M. Moncure, and J. G. Wood, "Burns: Pathophysiology of Systemic Complications and Current Management," *J. Burn Care Res.*, vol. 38, no. 1, pp. e469–e481, Jan. 2017.

[3] D. W. Mozingo, "Morbidity and Survival Probability in Burn Patients in Modern Burn Care," *Yearb. Surg.*, vol. 2016, no. 4, pp. 63–65, 2016.

[4] P. B. Sherren, J. Hussey, R. Martin, T. Kundishora, M. Parker, and B. Emerson, "Lethal triad in severe burns," *Burns*, 2014.

[5] G. D. Warden, "Burn Shock Resuscitation," pp. 16–23, 1992.

[6] M. Haberal, A. E. Sakallioglu Abali, and H. Karakayali, "Fluid management in major burn injuries," *Indian J. Plast. Surg.*, vol. 43, no. Suppl, pp. S29–S36, 2010.

[7] R. Cartotto and A. Zhou, "Fluid Creep: The Pendulum Hasn't Swung Back Yet!," *J. Burn Care Res.*, vol. 31, no. 4, pp. 551–558, Jul. 2010.

[8] L. Fodor, A. Fodor, Y. Ramon, O. Shoshani, Y. Rissin, and Y. Ullmann, "Controversies in fluid resuscitation for burn management: Literature review and our experience," *Injury*, vol. 37, no. 5, pp. 374–379, 2006.

[9] R. H. Demling, "The Burn Edema Process : Current Concepts," *J. Burn Care Rehabil.*, vol. 26, pp. 207–227, 2005.

[10] B. A. Latenser, "Critical care of the burn patient: The first 48 hours," *Crit. Care Med.*, vol. 37, no. 10, pp. 2819–2826, 2009.

[11] S. E. Wolf, J. K. Rose, M. H. Desai, J. P. Mileski, R. E. Barrow, and D. N. Herndon, "Mortality determinants in massive pediatric burns: An analysis of 103 children with ≤80% TBSA burns (≤70% full-thickness)," *Ann. Surg.*, vol. 225, no. 5, pp. 554–569, 1997.

[12] A. J. Diver, "The evolution of burn fluid resuscitation," vol. 6, pp. 345–350, 2008.

[13] N. Collis, G. Smith, and O. M. Fenton, "Accuracy of burn size estimation and subsequent fluid resuscitation prior to arrival at the Yorkshire Regional Burns Unit. A three year retrospective study,"

Burns, vol. 25, no. 4, pp. 345–351, 1999.

[14] M. B. Klein *et al.*, “The association between fluid administration and outcome following major burn: A multicenter study,” *Ann. Surg.*, vol. 245, no. 4, pp. 622–628, Apr. 2007.

[15] R. G. Carlson, R. K. Finley, S. F. Miller, L. M. Jones, M. A. Morath, and S. Alkire, “Fluid retention during the first 48 hours as an indicator of burn survival,” *J. Trauma - Inj. Infect. Crit. Care*, vol. 26, no. 9, pp. 840–844, 1986.

[16] M. Viceconti, C. Cobelli, T. Haddad, A. Himes, B. Kovatchev, and M. Palmer, “In silico assessment of biomedical products: The conundrum of rare but not so rare events in two case studies,” *Proc. Inst. Mech. Eng. Part H J. Eng. Med.*, vol. 231, no. 5, pp. 455–466, 2017.

[17] F. Pappalardo, G. Russo, F. M. Tshinanu, and M. Viceconti, “In silico clinical trials: concepts and early adoptions,” *Brief. Bioinform.*, vol. 20, no. April 2018, pp. 1699–1708, 2018.

[18] M. Viceconti, M. Juarez, C. Curreli, M. Pennisi, G. Russo, and F. Pappalardo, “POSITION PAPER: Credibility of In Silico Trial Technologies - A Theoretical Framing.,” *IEEE J. Biomed. Heal. informatics*, vol. 24, no. 1, pp. 4–13, 2019.

[19] O. Faris and J. Shuren, “An FDA viewpoint on unique considerations for medical-device clinical trials,” *New England Journal of Medicine*, vol. 376, no. 14. Massachussetts Medical Society, pp. 1350–1357, Apr-2017.

[20] G. Arturson, T. Groth, A. Hedlund, and B. Zaar, “Potential use of computer simulation in treatment of burns with special regard to oedema formation,” *Scand. J. Plast. Reconstr. Surg. Hand Surg.*, vol. 18, no. 1, pp. 39–48, 1984.

[21] A. Hedlund, B. Zaar, T. Groth, and G. Arturson, “Computer simulation of fluid resuscitation in trauma. I. Description of an extensive pathophysiological model and its first validation.,” *Computer methods and programs in biomedicine*, vol. 27. pp. 7–21, 1988.

[22] G. Arturson, T. Groth, A. Hedlundy, and B. Zaar, “Computer simulation of fluid resuscitation in trauma: First pragmatic validation in thermal injury,” *J. Burn Care Rehabil.*, vol. 10, no. 4, pp. 292–299, 1989.

[23] L. M. Roa, T. Gomez-Cia, and A. Cantero, “Analysis of burn injury by digital simulation,” *Burns*, vol. 14, no. 3, pp. 201–209, 1988.

[24] L. Roa Romero and T. Gomez Cia, “Analysis of the extracellular protein and fluid shifts in burned patients,” *Burns*, vol. 12, no. 5, pp. 337–342, 1986.

[25] L. Roa and T. Gómez-Cia, “A burn patient resuscitation therapy designed by computer simulation (BET). Part 1: simulation studies,” *Burns*, vol. 19, no. 4, pp. 324–331, 1993.

[26] J. L. Bert, B. D. Bowen, R. K. Reed, and R. K. R. Microvascular, “Microvascular exchange and interstitial volume regulation in the rat: model validation.”

[27] J. L. Bert, B. D. Bowen, X. Gu, T. Lund, and R. K. Reed, “Microvascular exchange during burn injury: II. Formulation and validation of a mathematical model,” *Circ. Shock*, vol. 28, pp. 199–219, 1989.

[28] J. L. Bert, B. D. Bowen, R. K. Reed, and H. Onarheim, “Microvascular exchange during burn injury: IV. Fluid resuscitation model,” *Circ. Shock*, vol. 34, pp. 285–297, 1991.

[29] S. L. Xie, R. K. Reed, B. D. Bowen, and J. L. Bert, “A Model of Human Microvascular Exchange,” *Microvascular Research*, vol. 49, no. 2. pp. 141–162, 1995.

[30] R. T. Ampratwum, B. D. Bowen, T. Lund, R. K. Reed, and J. L. Bert, “A model of fluid resuscitation following burn injury: formulation and parameter estimation,” *Comput. Methods Programs Biomed.*, vol. 47, no. 1, pp. 1–19, 1995.

[31] T. Lund, H. Onarheim, and R. K. Reed, “Pathogenesis of edema formation in burn injuries,” *World J. Surg.*, vol. 16, no. 1, pp. 2–9, 1992.

[32] Q. Huang, M. Zhao, and K. Zhao, “Alteration of vascular permeability in burn injury,” *Med. Express*, vol. 1, no. 2, pp. 62–76, 2014.

[33] H. Wiig and M. A. Swartz, “Interstitial fluid and lymph formation and transport: Physiological regulation and roles in inflammation and cancer,” *Physiological Reviews*, vol. 92, no. 3. pp. 1005–1060, Jul-2012.

[34] G. I. Elgjo, D. L. Traber, H. K. Hawkins, and G. C. Kramer, “Burn Resuscitation with Two Doses of 4 mL / kg Hypertonic Saline Dextran Provides Sustained Fluid Sparing : A 48-Hour Prospective Study in Conscious Sheep,” vol. 49, no. 2.

[35] G. C. Kramer, R. A. Gunther, M. L. Nerlich, S. S. Zweifach, and R. H. Demling, “Effect of dextran-70 on increased microvascular fluid and protein flux after thermal injury.,” *Circ. Shock*, vol. 9, no. 5, pp. 529–41, 1982.

[36] R. G. Hahn, “Volume Kinetics for Infusion Fluids,” *Anesthesiology*, vol. 113, no. 2, pp. 470–481, 2010.

[37] R. Bighamian, A. T. Reisner, and J. Hahn, “A Lumped-Parameter Subject-Specific Model of Blood Volume Response to Fluid Infusion,” *Front. Physiol.*, vol. 7, p. 390, 2016.

[38] B. K. Kataria *et al.*, “The Pharmacokinetics of Propofol in Children using Three Different Data Analysis Approaches,” *Anesthesiology*, vol. 80, pp. 104–122, 1994.

[39] A. Tivay, G. Arabi, D. Dor, R. Bighamian, G. C. Kramer, and J.-O. Hahn, “A Regularized System Identification Approach to Subject-Specific Physiological Modeling with Limited Data,” in *Proceedings of 2019 American Control Conference*, 2019, pp. 3468–3473.

[40] A. Tivay, X. Jin, A. Lo, C. G. Scully, and J.-O. Hahn, “Practical Use of Regularization in Individualizing a Mathematical Model of Cardiovascular Hemodynamics Using Scarce Data,” *Front. Physiol.*, vol. 11, p. Article 452, 2020.

[41] Q. Luo *et al.*, “Modeling Fluid Resuscitation by Formulating Infusion Rate and Urine Output in Severe Thermal Burn Adult Patients: A Retrospective Cohort Study,” *Biomed Res. Int.*, vol. 2015, p. Article 508043, 2015.

[42] V. K. Tiwari, “Burn wound: How it differs from other wounds,” *Indian Journal of Plastic Surgery*, vol. 45, no. 2. pp. 364–373, May-2012.

[43] M. Lehnhardt *et al.*, “A qualitative and quantitative analysis of protein loss in human burn wounds,” *Burns*, vol. 31, no. 2, pp. 159–167, 2005.

[44] H. J. Zdolsek, B. Kågedal, B. Lisander, and R. G. Hahn, “Glomerular filtration rate is increased in burn patients,” *Burns*, vol. 36, no. 8, pp. 1271–1276, Dec. 2010.

[45] M. E. Habib *et al.*, “Does Ringer Lactate Used in Parkland Formula for Burn Resuscitation Adequately Restore Body Electrolytes and Proteins?,” *Mod. Plast. Surg.*, vol. 07, no. 01, pp. 1–12, Jan. 2017.

[46] A. H. Øien and H. Wiig, “Modeling In Vivo Interstitial Hydration-Pressure Relationships in Skin and Skeletal Muscle,” *Biophys. J.*, vol. 115, no. 5, pp. 924–935, 2018.

[47] C. Chapple, B. D. Bowen, R. K. Reed, S. L. Xie, and J. L. Bert, “A model of human microvascular exchange: parameter estimation based on normals and nephrotics,” *Comput. Methods Programs Biomed.*, vol. 41, no. 1, pp. 33–54, 1993.

[48] M. A. Swartz, “The physiology of the lymphatic system,” *Advanced Drug Delivery Reviews*. 2001.

[49] G. H. J. Guyton, Arthur C, Taylor A.E, “Dynamics and Control of the Body Fluids,” in *Circulatory Physiology II:*, vol. 2, no. 17, 1985, p. Chapter 9.

[50] E. H. Bresler and L. J. Groome, “On equations for combined convective and diffusive transport of neutral solute across porous membranes.,” *Am. J. Physiol.*, vol. 241, no. 5, pp. F469-76, Nov. 1981.

[51] R. C. Blantz, A. Deng, C. M. Miracle, and S. C. Thomson, “Regulation of kidney function and metabolism: a question of supply and demand.,” *Trans. Am. Clin. Climatol. Assoc.*, vol. 118, pp. 23–43, 2007.

[52] W. R. Chenitz, B. A. Nevins, and N. K. Hollenberg, “Preglomerular resistance and glomerular perfusion in the rat and dog,” *Am. J. Physiol.*, vol. 231, no. 3, pp. 961–966, Sep. 1976.

[53] Guyton and Hall, “The Urinary System: Functional Anatomy and Urine Formation by the Kidneys,” in *Medical Physiology*, .

[54] Guyton and Hall, “Urine Formation by the Kidneys: II. Tubular Reabsorption and Secretion,” in *Medical Physiology*, .

[55] F. M. Toates and K. Oatley, “Computer simulation of thirst and water balance,” *Med. Biol. Eng.*, vol. 8, no. 1, pp. 71–87, 1970.

[56] F. M. Toates and K. Oatley, “Control of water-excretion by antidiuretic hormone: Some aspects of modelling the system,” *Med. Biol. Eng. Comput.*, vol. 15, no. 6, pp. 579–588, 1977.

[57] P. J. G. M. Voets and R. P. P. W. M. Maas, “Extracellular volume depletion and resultant hypotonic hyponatremia: A novel translational approach,” *Math. Biosci.*, vol. 295, no. May 2017, pp. 62–66, 2018.

[58] G. Baumann and J. F. Dingman, “Distribution, blood transport, and degradation of antidiuretic hormone in man,” *J. Clin. Invest.*, vol. 57, no. 5, pp. 1109–1116, 1976.

[59] H. HELLER and S. M. ZAIDI, “The metabolism of exogenous and endogenous antidiuretic hormone in the kidney and liver in vivo.,” *Br. J. Pharmacol. Chemother.*, vol. 12, no. 3, pp. 284–292, 1957.

[60] T. Lund, H. Onarheim, H. Wiig, and R. K. Reed, “Mechanisms behind increased dermal imbibition pressure in acute burn edema,” *Am. J. Physiol. - Hear. Circ. Physiol.*, vol. 256, no. 4, 1989.

[61] T. Lund, H. Wiig, and R. K. Reed, “Acute postburn edema: Role of strongly negative interstitial fluid pressure,” *Am. J. Physiol. - Hear. Circ. Physiol.*, vol. 255, no. 5, 1988.

[62] J. C. Ferguson, C. J. Martin, and C. Rayner, “Burn wound evaporation-measurement of body fluid loss by probe evaporimeter and weight change,” *Clin. Phys. Physiol. Meas.*, vol. 12, no. 2, pp. 143–155, May 1991.

[63] T. Namdar, P. L. Stollwerck, F. H. Stang, F. Siemers, P. Mailänder, and T. Lange, “Transdermal fluid loss in severely burned patients,” *GMS Ger. Med. Sci.*, vol. 8, pp. 6–10, 2010.

[64] R. M. Pitt, J. C. Parker, G. J. Jurkovich, A. E. Taylor, and P. W. Curreri, “Analysis of altered capillary pressure and permeability after thermal injury,” *J. Surg. Res.*, vol. 42, no. 6, pp. 693–702, 1987.

[65] J. Baudoin, P. Jafari, J. Meuli, L. A. Applegate, and W. Raffoul, “Topical negative pressure on burns: An innovative method for wound exudate collection,” *Plast. Reconstr. Surg. - Glob. Open*, vol. 4, no. 11, 2016.

[66] R. X. Xu, X. Sun, and B. S. Weeks, *Burns regenerative medicine and therapy*. Karger, 2004.

[67] F.-R. Curry, C. Michel, E. Renkin, and S. Geiger, “Mechanics and thermodynamics of transcapillary exchange.” Jan-1984.

[68] M. Jarzynska and M. Pietruszka, “The application of the Kedem-Katchalsky equations to membrane transport of ethyl alcohol and glucose,” *Desalination*, vol. 280, no. 1–3, pp. 14–19, 2011.

[69] D. J. Gillett and D. F. J. Halmagyi, “Results and limitations of blood volume measurements in sheep,” *J. Surg. Res.*, vol. 6, no. 5, pp. 211–214, May 1966.

[70] J. P. Coghlan, J. S. Fan, B. A. Scoggins, and A. A. Shulkes, “Measurement of extracellular fluid volume and blood volume in sheep.,” *Aust. J. Biol. Sci.*, vol. 30, no. 1–2, pp. 71–84, Apr. 1977.

[71] G. C. Kramer, B. A. Harms, R. A. Gunther, E. M. Renkin, and R. H. Demling, “The Effects of Hypoproteinemia on Blood-to-Lymph Fluid Transport in Sheep Lung,” 1981.

[72] Guyton and Hall, “Urine Formation by the Kidneys: I. Glomerular Filtration, Renal Blood Flow, and Their Control,” in *Medical Physiology*, .

[73] M. Nesje, A. Flåøyen, and L. Moe, “Estimation of glomerular filtration rate in normal sheep by the disappearance of iohexol from serum,” *Vet. Res. Commun.*, vol. 21, no. 1, pp. 29–35, 1997.

[74] Guyton and Hall, “The Body Fluid Compartments: Extracellular and Intracellular Fluids; Edem,” in *Medical Physiology*, .

[75] J. W. Bennett, “Regional body surface area of sheep,” *J. agric. Sci., Camb*, vol. 81, pp. 429–432, 2020.

[76] L. Kongstad, A. D. Möller, and P. O. Grände, “Reflection coefficient for albumin and capillary fluid permeability in cat calf muscle after traumatic injury,” *Acta Physiol. Scand.*, vol. 165, no. 4, pp. 369–377, Apr. 1999.

Fig. 1: Mathematical model to predict responses to burn injury and resuscitation. It includes volume kinetics to describe water volume and protein concentration in the vasculature and the tissues ("Plasma", "Burnt Tissues", "Intact Tissues", "Capillary wall", and "Tissue Surface"), renal function to describe UO response to vascular volume changes ("Kidneys"), and burn-induced perturbations in volume kinetics and renal function (denoted as "[a]" to "[f]"). J: water flow. Q: albumin flow. Subscripts: C (capillary filtration); L (lymph flow); F (fluid infusion); U (UO); RPF (renal plasma flow); EX (exudation); EV (evaporation); PD (protein denaturation); BT (burnt tissues); IT (intact tissues). [a]: Destruction of capillaries in burnt tissues. [b]: Denaturation of protein in burnt tissues. [c] Transient negative hydrostatic pressure in burnt tissues. [d]: Increased dermal fluid loss. [e]: Time-varying changes in capillary filtration and albumin transport. [f]: Vasodilation.

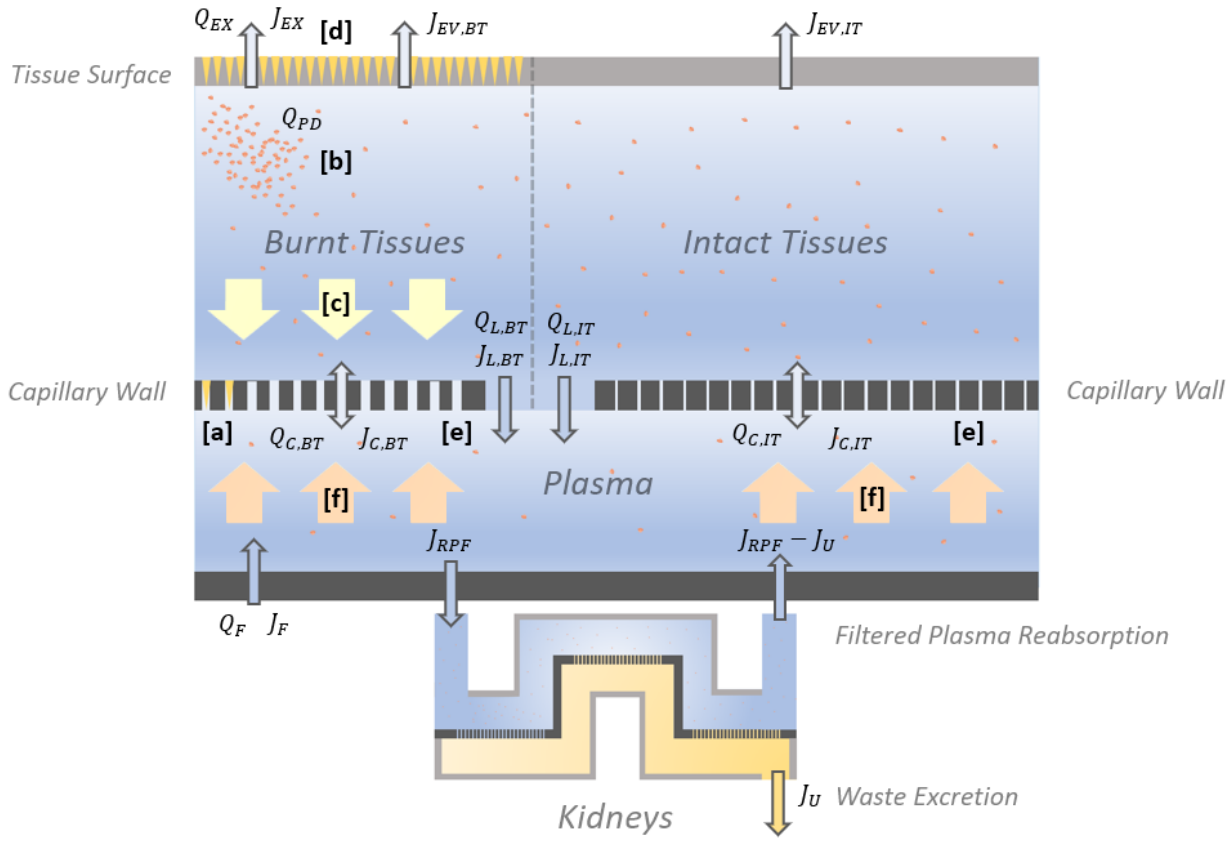

Fig. 2: Measured versus model-predicted plasma volume (PV) and urinary output (UO) responses of two 40kg sheep subject to 40% burn. Circles: measured responses. Solid lines: model-predicted responses. Dashed lines: measured fluid dose. (a) Sheep with PV resuscitated 200ml beyond pre-burn level 48 hours post-burn. (b) Sheep with PV resuscitated just up to pre-burn level 48 hours post burn.

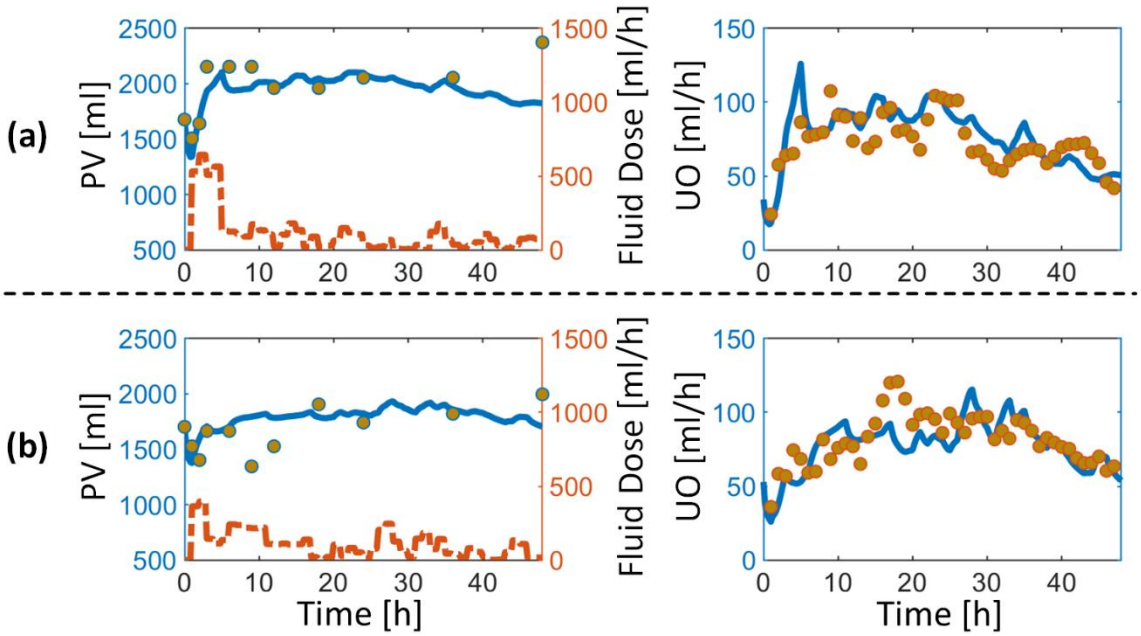

Fig. 3: Volume kinetic and renal function responses to burn injury and resuscitation predicted by population-average mathematical model. V: water volume. F_{ACC}: accumulated fluid. RF_{ADH}: reabsorption fraction due to ADH (see A.2). α: capillary pore radius ratio (see A.3). J_C: capillary filtration. Q_C: albumin transport across the capillary wall. J_L: lymphatic flow. In (b) and (d), blue solid, orange dash-dot, and brown dotted lines are plasma volume as well as burnt and intact tissue volumes, respectively. In (c), blue solid and orange dash-dot lines are accumulated resuscitation fluid volume and fluid creep, respectively. In (i)-(l), orange dash-dot and brown dotted lines correspond to burnt and intact tissues, respectively.

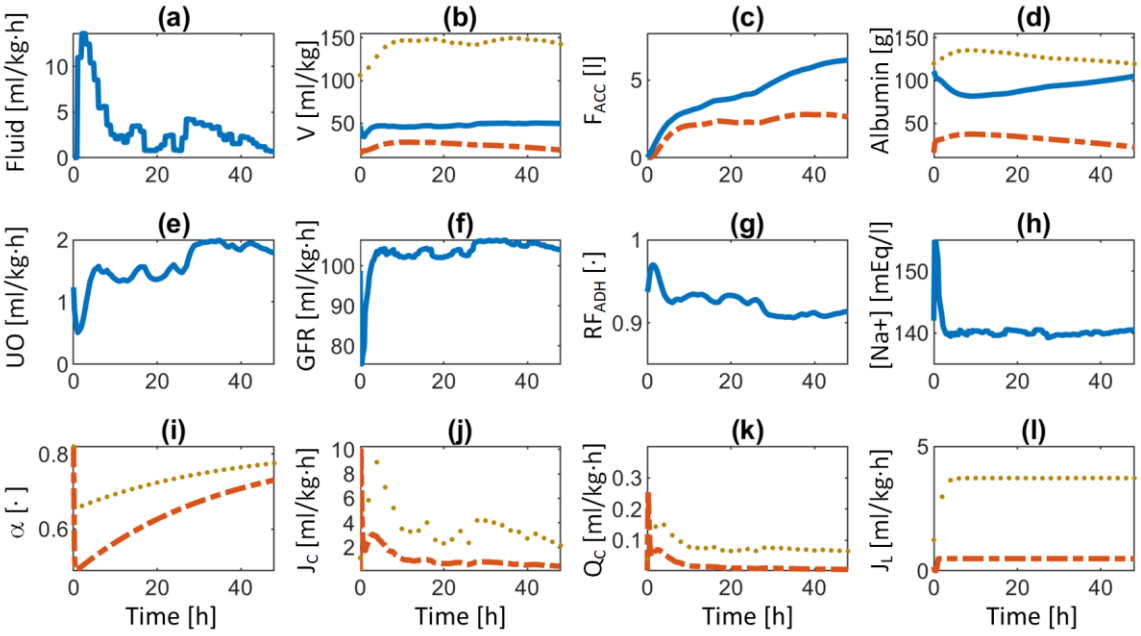

Fig. A1: Schematic of renal function model. J_{RPF}: renal plasma flow. J_{GFR}: glomerular filtration rate (GFR). $J_{RR,GT}$: reabsorption rate due to modulation of glomerulotubular balance. $J_{RR,ADH}$: reabsorption rate due to modulation of ADH. J_U: UO. R_G: hypothetical glomerular resistance modulating J_{RPF} against perturbations in plasma volume.

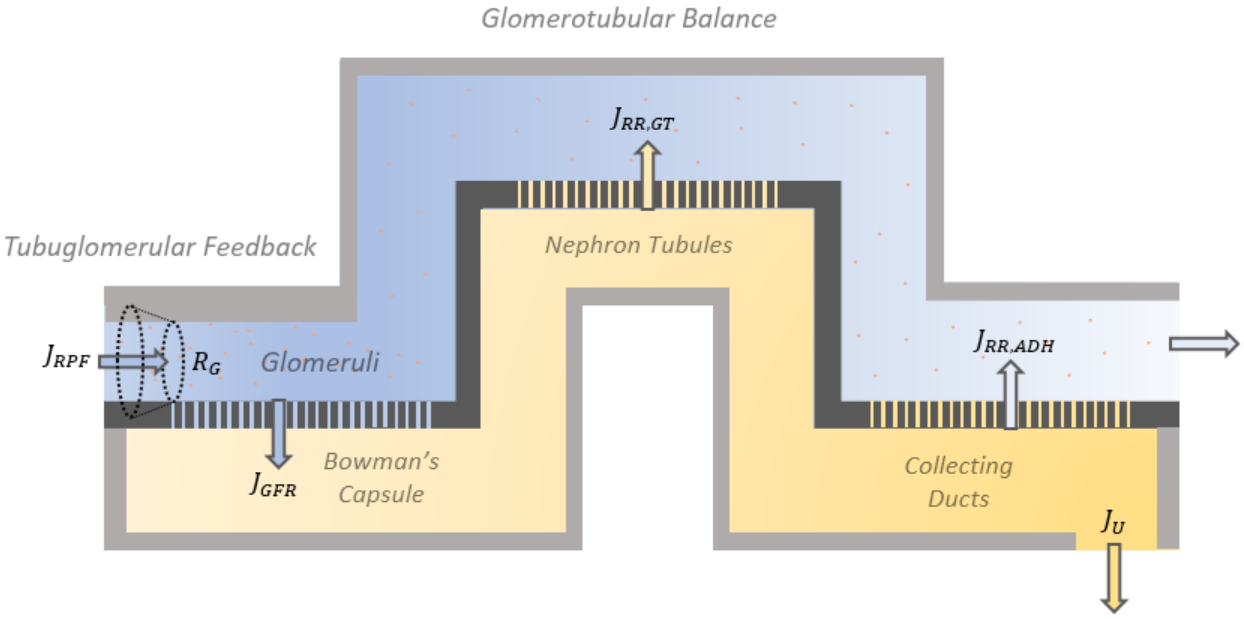

2020 American Control Conference
Denver, CO, USA, July 1-3, 2020

Virtual Patient Generation using Physiological Models through a Compressed Latent Parameterization

Ali Tivay, George C. Kramer, and Jin-Oh Hahn, *Senior Member, IEEE*

***Abstract*—This paper presents a data-driven approach to generating virtual patients using mathematical models of physiological processes. Such models often contain a large number of tunable parameters that must be calibrated to capture the observed characteristics of each real patient in a dataset. By sampling from this parameter space, potentially new virtual patients can be generated. However, it is often the case that the resulting set of virtual patients contains members that exhibit physiologically unrealistic behavior. In the present work, we employ a practically important case study on the modeling of cardiovascular responses to hemorrhage and fluid resuscitation in order to demonstrate that subject-specific characteristics observed in a dataset can be alternatively represented within a highly compressed latent parameter space without significant losses in calibration error for each real patient. Then, we show that by sampling from this latent parameter space, it is possible to generate new virtual patients that also exhibit physiologically realistic behavior.**

I. Introduction

The task of automating patient care using planning and control algorithms is worthy of extensive research attention due to its potential for achieving superiority in vigilant and precise performance of patient care routines, especially for critically ill patients. However, effective prototyping and testing of such algorithms are currently challenging due to the expensive nature and ethical limitations of conducting clinical trials on real patients.

Testing patient care algorithms based on populations of virtual patients is a promising direction that can potentially replace clinical trials in the early stages of algorithm and device development, increasing the maturity of the designs before they advance to more expensive stages of testing. For this purpose, using mathematical models of physiological processes as virtual patients has recently received notable attention in the research community [1]. To name a few: the diabetes simulator introduced in [2] is used to develop and test artificial pancreas control algorithms; the model of hemodynamic responses to hemorrhage presented in [3] has been used in a hardware-in-the-loop setup to test fluid resuscitation algorithms [4]; a synthetic virtual cohort of heart electro-grams has been used in [5] to run computer-aided clinical trials for implantable cardiac devices; and models of physiological responses to interacting drugs have been used in [6] to develop and test medication control algorithms. In addition, the U.S. Food and Drug Administration (FDA) has recently acknowledged the potential for computer simulations to complement regulatory submissions for new medical devices [7].

To reproduce the behavior of real patients in the form of virtual patients, a dynamic model of relevant physiological mechanisms is needed. Such models often consist of differential equations with possibly nonlinear elements and appropriately defined input-output signals, and a potentially large number of tunable parameters [8]–[10]. Generating virtual patients in this scenario consists of sampling from a distribution over the model parameters. A prevalent approach to conduct this sampling is to identify parameter values based on a dataset of subjects and use the identified models as virtual patients (e.g. as in [4], [11]). Alternatively, suitable physiological ranges for each parameter (calculated from the literature or based on the calibration of the model to a dataset) can be sampled to obtain potentially larger cohorts (e.g. as in [5], [12]). In some cases, additional information may be available about the distribution of each parameter and/or the relationship between the parameters, which can also be incorporated into the sampling procedure (e.g. as in [2], [13]). Furthermore, data "bootstrapping" can also be cited as a generation method, where subsets of data are randomly sampled and the corresponding maximum-likelihood parameter estimates are regarded as new virtual patients [14].

The possibility of generating virtual patients with realistic and reliable behavior through sampling from the parameter space of a model is limited by at least two important challenges: First, parameter values associated with a physiological system may be related in potentially unknown ways, and thus breaking relations by independently sampling from each model parameter could create virtual patients that would not have existed in reality. Second, a vast array of mathematical models proposed in biology and physics are known to exhibit the "sloppiness" property [15] (i.e., a lack of practical identifiability [16], [17]) in many directions in their parameter space, which is known to cause parameter estimates to drift out of proportion during model calibration, giving larger-than-reality values for parameter ranges, which can in turn result in unrealistic virtual patients when sampled. As an effective ad-hoc solution, objectively un-realistic simulations can be omitted from a virtual population after sampling from the parameters [18], however, a systematic way of generating virtual patients that takes into account both parameter interactions and parameter sloppiness is desirable.

In an attempt to address this challenge, we investigate the generation of virtual patients through sampling from a compressed latent parameter space for the model, where both parameter interaction and sloppiness are minimal. Focusing on a practically important case study on the physiological modeling of cardiovascular responses to hemorrhage and fluid resuscitation, a model structure is first presented that

*Research supported by National Science Foundation CAREER Award (Grant No. 1748762), and CDMRP (Grant No. W81XWH-19-1-0322).

A. Tivay and J.O. Hahn are with the Mechanical Engineering Department, University of Maryland, College Park, MD 20742 USA (phone: 301-405-7864; fax: 301-314-9477; e-mail: tivay@umd.edu).

G. Kramer is with the Anesthesiology Department, University of Texas Medical Branch, Galveston, TX 77555 USA.

978-1-5386-8266-1/$31.00 ©2020 AACC

can be used to simulate changes in blood hematocrit (HCT), cardiac output (CO), and mean arterial pressure (MAP) in response to hemorrhage and fluid resuscitation. Then, using patient-specific data available for HCT, CO, and MAP over time, the parameters of the model can be calibrated to match its behavior to each real patient. For this purpose, we introduce a compressed latent parameter space for the model where variabilities across different patients are represented by variations in a few latent directions, without significant losses in calibration error. Then, we demonstrate that it is possible to generate new virtual patients that exhibit realistic behavior by sampling from this latent parameter space.

II. Case Study: Modeling Cardiovascular Responses to Hemorrhage and Fluid Resuscitation

Hemorrhage (bleeding) is a serious event that can be incident in critical patients and patients subjected to trauma, the effects of which can be counteracted with appropriate fluid resuscitation. To generate virtual patients that can help design and test automated fluid resuscitation algorithms, a dynamic model is needed to represent the macroscopic responses of the cardiovascular system to both hemorrhage and fluid resuscitation. In this section, we present such a model structure.

Fig. 1 shows a schema of the proposed model structure for the macroscopic response of the cardiovascular system to fluid perturbation. We consider the following equations for the exchange and balance of fluid volume in the system:

$$\dot{v}_a = Q - (p_a - p_v)/R - J_h - J_f \quad (1)$$

$$\dot{v}_v = -Q + (p_a - p_v)/R + J_i \quad (2)$$

$$\dot{v}_r = -J_h H \quad (3)$$

$$H = v_r/(v_a + v_v) \quad (4)$$

$$V = v_a + v_v \quad (5)$$

where v_a and v_v denote arterial and venous blood volume, V is the total blood volume, v_r is the total volume of red blood cells, H represents hematocrit, p_a and p_v denote MAP and central venous pressure (CVP), R represents the systemic vascular resistance, Q is the cardiac output, J_h is the flow rate of hemorrhage, J_f is the flow rate of fluid exchange with the interstitial compartment, and J_i is the flow rate of fluid infusion into the bloodstream.

Changes in MAP and CVP are modeled to linearly depend on changes in arterial and venous blood volume through elastance parameters as follows:

$$\Delta p_a = K_a \Delta v_a \quad (6)$$

$$\Delta p_v = K_v \Delta v_v \quad (7)$$

where K_a and K_v represent the elastance of the arterial and venous volume compartments respectively, and $\Delta x = x\text{-}x_0$ for all quantities.

The blood volume compartment is known to be in relative equilibrium with the fluid in its surrounding tissue (called the interstitial compartment). A perturbation in blood volume is partially counteracted by a shift of fluid to/from this tissue compartment. The net rate of fluid shift J_f is thus

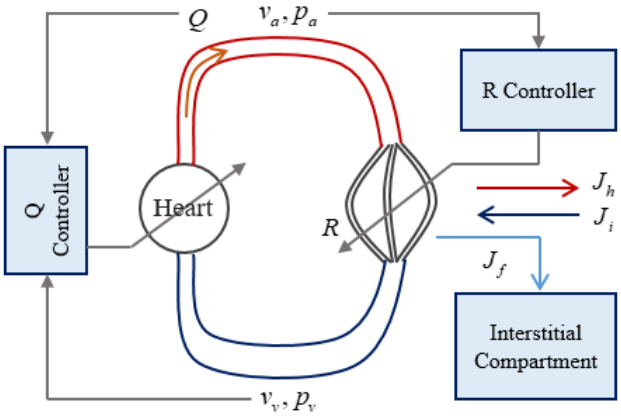

Figure 1. Schematic illustration of the proposed model of cardiovascular response to hemorrhage and fluid resuscitation

modeled as the control input of a hypothetical controller that has the goal of maintaining total blood volume as follows:

$$J_f = -K_p(r_V - \Delta V) \quad (8)$$

$$r_V = \frac{1}{1+\alpha_i}\int_0^t J_i(\tau)d\tau - \frac{1}{1+\alpha_h}\int_0^t J_h(\tau)d\tau \quad (9)$$

where K_p is a proportional gain for the controller, and r_v is the new value of blood volume after re-equilibrium. This value depends on the history of fluid perturbations, and parameters α_i and α_h determine the fraction of each perturbation that will be compensated for by a shift of fluid to/from the tissue compartment. Please refer to [19] for more information about this particular formulation.

The systemic vascular resistance (SVR) denoted by R represents the resistance to blood flow that is present throughout the vascular system. The body can change this resistance through vasoconstriction and vasodilation to restore a lower-than-normal MAP [20]. Also, a change in the fraction of red blood cells in the blood (H) directly affects blood viscosity, which in turn affects SVR [21]. The change in resistance (ΔR) is therefore modeled as a control input that has the goal of maintaining a normal MAP, and is also disturbed by changes in H as follows:

$$\Delta R = -\frac{K_r}{\tau_r s + 1}\Delta p_a + K_h \Delta H \quad (10)$$

where the parameters K_r and τ_r are the gain and time constant of the controller respectively, and K_h represents the sensitivity of SVR to changes in hematocrit.

The cardiac output denoted by Q is the flow rate of blood that is pumped by the heart. This flow rate can be affected by a few important mechanisms: The Frank-Starling mechanism is related to the inherent properties of cardiac muscles, where a higher preload (~proportional to p_v) results in a more forceful stroke in a single beat and thus higher Q. The cardiac contractility (force of contraction) and heart rate are controlled by the autonomic nervous system and the endocrine system in order to maintain a normal Q [20]. Overall, to obtain a minimal and lumped model of these

effects, Q is assumed to be regulated as a controlled variable by a controller that acts through manipulating a control input (which corresponds to heart rate and cardiac contractility), and is disturbed by changes in preload (Δp_v) as follows:

$$\Delta Q = \frac{s}{s + K_c}\left(\beta_v \Delta p_v\right) \tag{11}$$

where K_c is the controller gain, and β_v is the sensitivity of cardiac output to changes in preload (which corresponds to the slope of the cardiac function curve in the Frank-Starling mechanism). Note that (11) represents the closed-loop relationship between the disturbances and ΔQ.

To numerically simulate the model, the initial values for arterial and venous blood volume are set as $v_{a0}=0.3V_0$, and $v_{v0}=0.7V_0$, where V_0 is the initial total blood volume to be estimated; the values for initial arterial pressure p_{a0}, initial venous pressure p_{v0}, initial blood hematocrit H_0, and initial cardiac output Q_0 are set from baseline values in measured data; and the initial SVR is calculated from $R_0=(p_{a0}-p_{v0})/Q_0$.

In the presented model structure, each subject can be characterized by $n_p=11$ tunable parameters (denoted hereafter by the vector θ) as follows:

$$\theta = \left[\alpha_i \;\; \alpha_h \;\; K_p \;\; V_0 \;\; K_a \;\; K_v \;\; K_r \;\; \tau_r \;\; K_h \;\; \beta_v \;\; K_c\right] \tag{12}$$

The experimental data used in this work included HCT, CO, and MAP time-series measurements acquired from $N=23$ animal (sheep) experiments under hemorrhage and fluid resuscitation [22], [23]. The measurements were made at ~5 min intervals for 180 minutes.

III. Virtual Patient Generation using a Compressed Latent Parameterization

An important desirable when generating virtual patients is for the variations in the generated set to be representative of variations that are incident across real patients. Such a representation for inter-subject variability can be thought of as a joint distribution over the model parameters, where each sample represents a virtual patient. In the absence of additional assumptions, finding such a joint distribution is often infeasible given the amount of data that is available in physiological applications. In this section, we first argue that when certain conditions are met, the variations across real subjects can be alternatively represented in a compressed latent parameter space for the model. Then, we demonstrate that independently sampling from the dimensions of this latent space results in a set of generated patients that can represent the variations observed in the dataset and also exhibit realistic behavior.

A. Model Calibration in Compressed Latent Space

To find a compressed representation for the variabilities across patients (in case such a representation exists), we first consider a nominal model parameter vector $\bar{\theta}$, which represents a model of typical physiological behavior. One candidate for such a model is the "group-average" model, which is defined as the solution to the following optimization problem:

$$\bar{\theta} = \arg\min_{\theta} \left\| \mathbf{Y} - \hat{\mathbf{Y}}(\theta) \right\|_2^2 \tag{13}$$

where $\mathbf{Y}$ denotes the data from *all* patients and $\hat{\mathbf{Y}}(\theta)$ denotes the corresponding model predictions given the parameter θ. The solution $\bar{\theta}$ is a maximum-likelihood estimate using all available data, which can be interpreted as a group-average model that represents expected behavior in the population.

Given the group-average model $\bar{\theta}$, variations across real patients in the dataset can be thought of as local deviations from $\bar{\theta}$. To find a potentially compressed representation for these deviations, we are interested in finding orthogonal directions in the vicinity of $\bar{\theta}$, sorted by the prominence of their effect on the predictions of the model. To find such directions, $k >> n_p$ random local *deviations* around $\bar{\theta}$ are obtained and stored in Θ ($n_p \times k$). The corresponding *changes* in model predictions are stored in $\hat{\mathbf{Y}}_\Theta$ ($n_d \times k$). Then, the following matrix can be constructed:

$$\mathbf{C} = \hat{\mathbf{Y}}_{\boldsymbol{\Theta}} \boldsymbol{\Theta}^{\mathbf{T}} = \mathbf{U}\mathbf{S}\mathbf{V}^{\mathbf{T}} \tag{14}$$

where the elements of $\mathbf{C}$ represent the (scaled) covariance between local parametric deviations from the group-average model and the corresponding changes in model predictions. The matrices $\mathbf{U}$, $\mathbf{S}$, and $\mathbf{V}$ are computed from the singular value decomposition of the covariance matrix. The columns of $\mathbf{V}$ constitute sorted orthogonal directions of maximum covariance in the parameter space, and the diagonal values of $\mathbf{S}$ represent the local sensitivity of model predictions to deviations along each of the columns of $\mathbf{V}$.

Depending on the structure of the physiological model, the matrix of (sorted) local sensitivities $\mathbf{S}$ can show interesting properties. For example, in the case that the proposed model exhibits the sloppiness property [15] (which is a prevalent property in a wide range of proposed models across many disciplines) the first few elements of $\mathbf{S}$ will be significantly larger than the rest. This means that locally deviating from the group-average model $\bar{\theta}$ in the first few directions in $\mathbf{V}$ will have a large effect on model outputs while deviating from $\bar{\theta}$ in the last few directions in $\mathbf{V}$ will have a small effect on model outputs and possibly only affect the internal behavior of the model.

Based on the observation above, we can define the following model calibration problem to find patient-specific models for each member of the dataset without unnecessary deviations from the group-average model:

$$\hat{\theta}_i = \arg\min_{\theta} \left\| \mathbf{Y_i} - \hat{\mathbf{Y}}(\theta) \right\|_2^2 + \lambda \left\| (\theta - \bar{\theta})^T \mathbf{V} \right\|_1 \tag{15}$$

where $\hat{\theta}_i$ denotes the vector of model parameters calibrated to match the behavior of real patient i. The second term in (15) measures the L_1-deviation of each patient from the group-average model in the latent space ($\phi^T = \theta^T\mathbf{V} - \bar{\theta}^T\mathbf{V}$). The well-known sparsity-promoting nature of the L_1-norm

induces compression in the latent space so that individual subjects deviate from $\bar{\theta}$ only in a few necessary latent directions. The rate of compression can be controlled through the choice of λ.

B. Generating Virtual Patients

Assuming that a compressed representation exists in the latent space ϕ for variations across different subjects, it is possible to generate new in-silico subjects by mimicking the observed variations in the latent space through sampling from the latent parameters. In this work, samples are drawn from a distribution of the mean-field variational family:

$$P(\phi) = \prod_{j=1}^{n_p} p(\phi_j) \tag{16}$$

where each dimension of the latent parameter space ϕ_j has its density $p(\phi_j)$. For each latent dimension, we use a uniform density with a range that is equal to that of the real patients represented in the compressed latent space. Sampling from $P(\phi)$ will generate virtual patients, and the corresponding model parameter values can be obtained from:

$$\theta = V\phi + \bar{\theta} \tag{17}$$

C. Comparing Generated Cohorts

To evaluate and compare different generated cohorts of virtual patients in terms of having realistic members and covering the range of variation observed in the real patient dataset, we first define the following evidence for the real patient i:

$$P(\mathbf{Y_i} \mid \mathbf{I_i}) = \int_{\Phi} P(\mathbf{Y_i} \mid \mathbf{I_i}, \phi) P(\phi) d\phi \tag{18}$$

where $P(\mathbf{Y_i}|\mathbf{I_i})$ represents the probability that the generation method $P(\phi)$ produces patients that behave similarly to the measured data from the actual subject i, when given the input signals that subject i received in reality (I_i). In this setting, the similarity between a virtual patient and a real patient is measured by measuring the distance of their outputs through a Gaussian kernel:

$$P(\mathbf{Y_i} \mid \mathbf{I_i}, \phi) = \frac{\exp\left(-\frac{1}{2}(\mathbf{Y_i} - \hat{\mathbf{Y}}(\phi))^T \mathbf{\Sigma}^{-1} (\mathbf{Y_i} - \hat{\mathbf{Y}}(\phi))\right)}{\sqrt{(2\pi)^{n_d} |\mathbf{\Sigma}|}} \tag{19}$$

where the elements of the diagonal matrix $\mathbf{\Sigma}$ determine how close the simulation and the data should be to be considered similar. In the present work, diagonal elements of Σ were chosen according to the type of each data point (i.e., σ_{MAP} for MAP data, σ_{HCT} for HCT data, and σ_{CO} for CO data).

Having the probability in (18), which represents how likely is the incidence of patient i under the generation method $P(\phi)$, we can construct the following overall score:

$$S = -\log\left(\prod_{i=1}^{N} P(\mathbf{Y_i} \mid \mathbf{I_i})\right) = -\sum_{i=1}^{N} \log\left[P(\mathbf{Y_i} \mid \mathbf{I_i})\right] \tag{20}$$

which represents how likely is the incidence of *all* real patients under the generation method $P(\phi)$. The score S will be used in subsequent sections as one of the ways to compare different generated cohorts, and a lower score shows a better cohort in this sense.

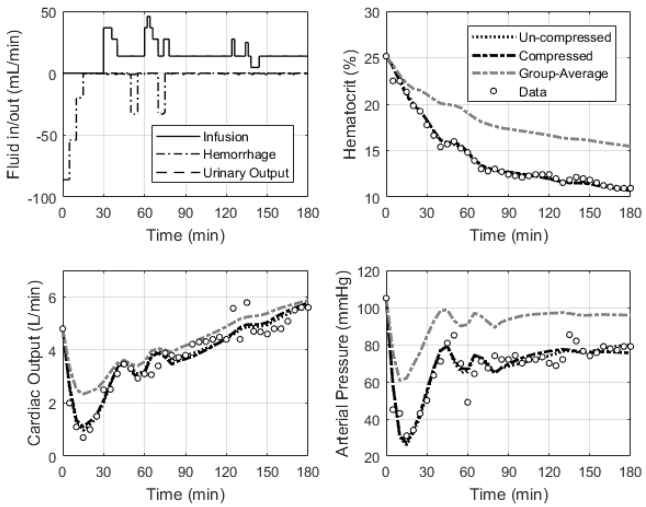

Figure 2. Simulation results of the compressed, un-compressed and group-average models versus the data for one representative subject.

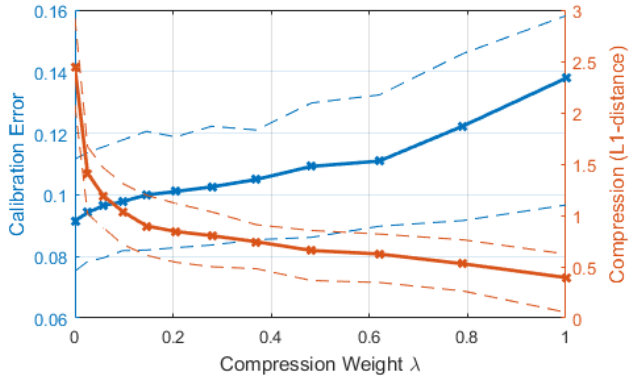

Figure 3. The effect of parameter space compression on calibration error (blue) and L_1-distance (red). Solid lines denote the mean value across all subjects, and dashed lines denote first and third quartile values.

IV. Results and Discussion

Fig. 2 shows the HCT, CO, and MAP responses of the uncompressed, compressed, and group-average calibrated models versus the data for a representative subject. The responses of the group-average model follow the overall trends observed in the data but do not exactly match the data, as this kind of model represents the expected behavior in the population. Uncompressed calibration (λ=0) of model parameters to the subject-specific data results in responses that match the data well. Alternatively, compressed calibration (λ=0.15) of the model to this data results in responses that match the data well and are close to the uncompressed case. This indicates that it is possible to calibrate the model to subject-specific data by limited deviations from the group-average model.

Fig. 3 shows changes in calibration error and deviation distance (in the L_1 sense, from the group-average model)

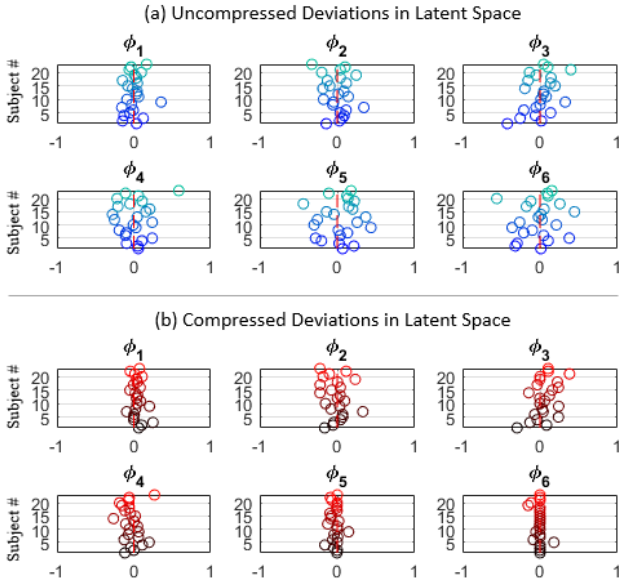

Figure 4. Comparison of the first six latent parameter values identified for the dataset of 23 subjects: (a) latent parameter values in the uncompressed case where λ=0, and (b) in the compressed case where λ=0.15.

with respect to the compression weight λ for the subjects in the dataset. In the uncompressed case (λ=0), the calibrated parameter values tend to have very high L_1-distances from the group-average model, which indicates that they are highly dispersed in the parameter space. As λ is increased, deviation distances drop with a steep slope, while at the same time calibration errors only mildly increase. Furthermore, in the case that λ is increased to very high values, calibration errors will increase significantly and tend to the calibration error for the group-average model. This indicates that for a middle-ground value of the compression weight (e.g. λ=0.15) the variations across different subjects can be represented in a compressed way without noticeable losses in calibration error.

Fig. 4 shows values for the first six latent parameters in case of uncompressed and compressed calibration. In Fig. 4(a), which represents the uncompressed calibration case, variations are visible in all dimensions of the latent space. However, in the compressed calibration case shown in Fig. 4(b), most of the variations are represented by the first four dimensions of the latent space, while from the fifth dimension onward, the latent parameters are nearly zero for most of the real subjects. This result suggests that the variations across different subjects have a compressed representation in the latent space.

Fig. 5 compares the outcomes of virtual subject generation when the compressed versus uncompressed latent parameter values are used in (16) to generate subjects. These outcomes have been shown as histograms of model output values at three points in time (20min, 45min, and 95min) in response to a typical hemorrhage and resuscitation profile. In the uncompressed case, objectively un-realistic subjects are incident (and even common) in the set: (i) many virtual

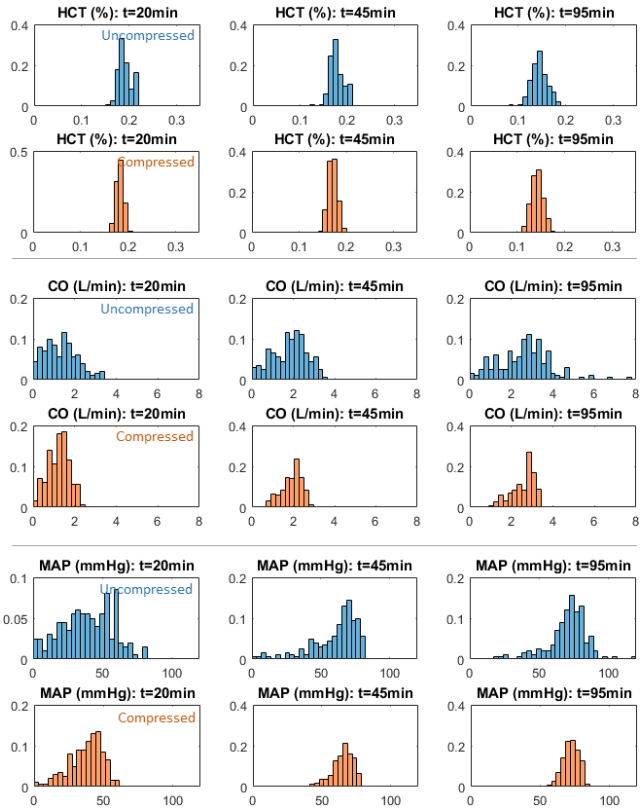

Figure 5. Representative histograms of the HCT, CO, and MAP responses from the virtual subjects: the comparison is made between subjects that were generated using compressed vs uncompressed parameter values.

subjects have a CO at or near zero at t=20min, and similarly, (ii) many have a MAP near zero at t=20min, and (iii) some virtual subjects have a cardiac output greater than 5 at t=95min, which is also considered un-realistic. Interestingly, in the compressed case, most of these un-realistic subjects vanish from the generated population. The potential reason behind this advantage is the following: In the uncompressed calibration case, the sloppiness property [15] of the model structure with respect to available data causes unnecessary drifts in some parametric directions (visible in Fig. 4(a) and also Fig. 3 at λ=0). A sampling method that uses these values would also sample in-between the drifted values and thus create un-realistic virtual subjects. In contrast, latent space compression prevents any such unnecessary deviations from the group-average model, resulting in a lower number of un-realistic virtual subjects.

Fig. 6 compares the quality of the generated cohort for different compression weights, using the score introduced in equation (20). At λ=0, where there is no compression, the score shows a poor value, which indicates that the probability of generating realistic (as compared to the data) patients in the uncompressed case is relatively low. As λ increases above zero, the score improves, which corresponds to using the compressed method for virtual patient generation. Finally, for large values of λ, most generated virtual patients will become too similar to the group-average

model, which again results in a poor score. As a result, it is beneficial to pick a moderate compression weight according to Fig. 3 for the purpose of model calibration and virtual subject generation.

V. Conclusion

In this paper, we investigated the data-driven generation of virtual patients using physiological models. For this purpose, a parameter space compression method and a virtual patient generation method were proposed and applied to a practically important case study on the physiological modeling of cardiovascular responses to hemorrhage (bleeding) and fluid resuscitation. The results suggested the validity of the proposed approach: A set of virtual patients generated using the proposed compressed sampling method showed higher similarity to a real dataset when compared to the uncompressed sampling case. Furthermore, unlike the uncompressed sampling case, the compressed sampling method generated fewer virtual patients with unrealistic behavior. Future effort should be devoted to the investigation of the advantages and limitations of the proposed method for a wider range of physiological modeling applications, and to the possibility of utilizing more advanced calibration and compression techniques to further improve the quality of the generated virtual patients.

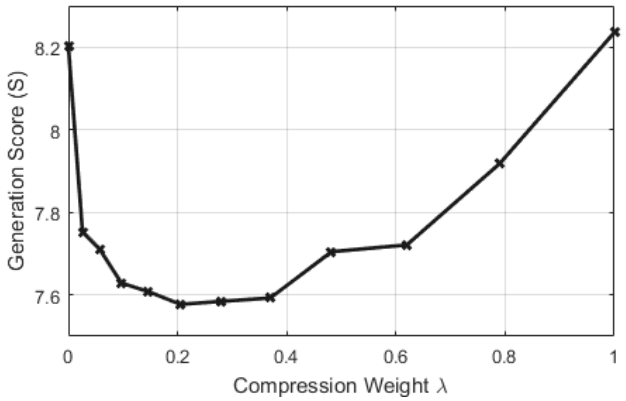

Figure 6. The quality of virtual subjects generated by sampling from a compressed latent space with compression weight λ (lower is better).

References

[1] F. Pappalardo, G. Russo, F. M. Tshinanu, and M. Viceconti, "In silico clinical trials: concepts and early adoptions," *Brief. Bioinform.*, Jun. 2018.

[2] C. D. Man, F. Micheletto, D. Lv, M. Breton, B. Kovatchev, and C. Cobelli, "The UVA/PADOVA Type 1 Diabetes Simulator: New Features.," *J. Diabetes Sci. Technol.*, vol. 8, no. 1, pp. 26–34, Jan. 2014.

[3] R. Bighamian, B. Parvinian, C. G. Scully, G. Kramer, and J.-O. Hahn, "Control-oriented physiological modeling of hemodynamic responses to blood volume perturbation.," *Control Eng. Pract.*, vol. 73, no. April 2018, pp. 149–160, Apr. 2018.

[4] H. Mirinejad *et al.*, "Evaluation of Fluid Resuscitation Control Algorithms via a Hardware-in-the-Loop Test Bed," *IEEE Trans. Biomed. Eng.*, pp. 1–1, 2019.

[5] K. Jang *et al.*, "Computer Aided Clinical Trials for Implantaule Cardiac Devices," in *2018 40th Annual International Conference of the IEEE Engineering in Medicine and Biology Society (EMBC)*, 2018, pp. 1–4.

[6] X. Jin and J.-O. Hahn, "Semi-adaptive switching control for infusion of two interacting medications," *Biomed. Signal Process. Control*, vol. 43, pp. 183–195, May 2018.

[7] O. Faris and J. Shuren, "An FDA Viewpoint on Unique Considerations for Medical-Device Clinical Trials," *N. Engl. J. Med.*, vol. 376, no. 14, pp. 1350–1357, Apr. 2017.

[8] R. Moss, T. Grosse, I. Marchant, N. Lassau, F. Gueyffier, and S. R. Thomas, "Virtual patients and sensitivity analysis of the Guyton model of blood pressure regulation: Towards individualized models of whole-body physiology," *PLoS Comput. Biol.*, vol. 8, no. 6, Jun. 2012.

[9] A. Mousavi, A. Tivay, B. Finegan, M. S. McMurtry, R. Mukkamala, and J.-O. Hahn, "Tapered vs. Uniform Tube-Load Modeling of Blood Pressure Wave Propagation in Human Aorta," *Front. Physiol.*, vol. 10, no. JUL, p. 974, Aug. 2019.

[10] M. Doosthosseini, E. Hansen, and H. K. Fathy, "On the accuracy of drug-resistant cell population estimation from total cancer size measurements," in *2019 18th European Control Conference, ECC 2019*, 2019, pp. 343–350.

[11] M. Davidian and D. M. Giltinan, "Nonlinear models for repeated measurement data: An overview and update," *J. Agric. Biol. Environ. Stat.*, vol. 8, no. 4, pp. 387–419, Dec. 2003.

[12] D. Brown *et al.*, "Trauma in silico: Individual-specific mathematical models and virtual clinical populations," *Sci. Transl. Med.*, vol. 7, no. 285, p. 285ra61-285ra61, 2015.

[13] A. Haidar, M. E. Wilinska, J. A. Graveston, and R. Hovorka, "Stochastic Virtual Population of Subjects With Type 1 Diabetes for the Assessment of Closed-Loop Glucose Controllers," *IEEE Trans. Biomed. Eng.*, vol. 60, no. 12, pp. 3524–3533, Dec. 2013.

[14] S. Barish, M. F. Ochs, E. D. Sontag, and J. L. Gevertz, "Evaluating optimal therapy robustness by virtual expansion of a sample population, with a case study in cancer immunotherapy," *Proc. Natl. Acad. Sci.*, vol. 114, no. 31, pp. E6277–E6286, Aug. 2017.

[15] M. K. Transtrum, B. B. Machta, K. S. Brown, B. C. Daniels, C. R. Myers, and J. P. Sethna, "Perspective: Sloppiness and emergent theories in physics, biology, and beyond," *J. Chem. Phys.*, vol. 143, no. 1, p. 010901, Jul. 2015.

[16] A. Raue *et al.*, "Structural and practical identifiability analysis of partially observed dynamical models by exploiting the profile likelihood," *Bioinformatics*, vol. 25, no. 15, pp. 1923–1929, Aug. 2009.

[17] A. Tivay, G. Arabi Darreh Dor, R. Bighamian, G. C. Kramer, and H. Jin-Oh, "A Regularized System Identification Approach to Subject-Specific Physiological Modeling with Limited Data," in *2019 American Control Conference (ACC)*, 2019, pp. 3468–3473.

[18] P. Pathmanathan, J. M. Cordeiro, and R. A. Gray, "Comprehensive Uncertainty Quantification and Sensitivity Analysis for Cardiac Action Potential Models.," *Front. Physiol.*, vol. 10, p. 721, 2019.

[19] R. Bighamian, A. T. Reisner, and J. Hahn, "A Lumped-Parameter Subject-Specific Model of Blood Volume Response to Fluid Infusion," *Front. Physiol.*, vol. 7, p. 390, 2016.

[20] J. E. (John E. Hall, *Guyton and Hall textbook of medical physiology*. .

[21] Y. Çınar, G. Demir, M. Paç, and A. B. Çınar, "Effect of hematocrit on blood pressure via hyperviscosity," *Am. J. Hypertens.*, vol. 12, no. 7, pp. 739–743, Jul. 1999.

[22] A. D. Rafie *et al.*, "Hypotensive Resuscitation of Multiple Hemorrhages Using Crystalloid and Colloids," *Shock*, vol. 22, no. 3, pp. 262–269, Sep. 2004.

[23] S. U. Vaid *et al.*, "Normotensive and hypotensive closed-loop resuscitation using 3.0% NaCl to treat multiple hemorrhages in sheep," *Crit. Care Med.*, vol. 34, no. 4, pp. 1185–1192, Apr. 2006.

Development and Evaluation of a Mathematical Model of Volume Kinetics and Renal Function after Burn Injury and Resuscitation

Ghazal A. DarrehDor[1], Ali Tivay[1], Ramin Bighamian[2], Chris Meador[3], George C. Kramer[3,4]
Jin-Oh Hahn[1†], Jose Salinas[5]

[1]: Department of Mechanical Engineering, University of Maryland

[2]: U.S. Food and Drug Administration

[3]: Arcos, Inc.

[4]: Department of Anesthesiology, University of Texas Medical Branch

[5]: U.S. Army Institute of Surgical Research

[†]: Corresponding Author

Disclaimer

This article reflects the views of the author and should not be construed to represent FDA's views or policies.

Abstract

We developed and evaluated the validity of a mathematical model of blood volume (BV) kinetics and renal function (RF) in response to burn injury and resuscitation, which is applicable to the development and non-clinical testing of burn resuscitation protocols and algorithms. Prior mathematical models of burn injury and resuscitation are not ideally suited to such applications due to their limited credibility in predicting BV and urinary output (UO) observed in a wide range of burn patients as well as in incorporating contemporary knowledge of burn pathophysiology. Our mathematical model consists of a multi-compartmental model of BV kinetics, a hybrid mechanistic-phenomenological model of RF, and novel lumped-parameter models of burn-induced perturbations in BV kinetics and RF equipped with contemporary knowledge on burn-related physiology and pathophysiology. Using the dataset collected from 16 sheep and 156 burn patients, we showed that our mathematical model can be characterized with physiologically plausible parameter values to accurately predict BV kinetic and RF responses to burn injury and resuscitation on an individual basis against a wide range of pathophysiological variability. In particular, the normalized mean absolute error associated with our UO prediction (18 +/-5.5 %) was considerably smaller than a recently reported black-box model[1] (30+/-6%) while the underlying UO variability was much larger in our dataset (69% versus 38% in terms of the coefficient of variation). In addition, despite its structural complexity, our mathematical model could be individualized to a patient by personalizing only 4 cardinal parameters. Its promising predictive performance combined with amenity for efficient individualization suggest that our mathematical model may serve as an effective basis for

the development and non-clinical evaluation of patient-specific burn resuscitation protocols and algorithms.

1. Luo, Q. *et al.* Modeling fluid resuscitation by formulating infusion rate and urine output in severe thermal burn adult patients: A retrospective cohort study. *BioMed Research International* **2015**, (2015).

Learning Objectives

1. Understand the potential of mathematical models of physiological systems as a basis for the development and testing of treatment protocols as well as the training of medical personnel

2. Understand the requirement for a mathematical model of burn injury and resuscitation whose intended use is the development and testing of burn resuscitation protocols as well as the training of medical personnel

3. Understand the blood volume kinetic and renal function responses to burn injury and burn resuscitation and a mathematical model to represent those responses

Funding

This research was supported in part by the U.S. Army SBIR Program (Award No. W81XWH-16-C-0179), the Congressionally Directed Medical Research Programs (Award No. W81XWH-19-1-0322), and the U.S. National Science Foundation CAREER Award (Award No. 1748762).